

1    **Nature Behind Multiple Populations of Extrasolar Gaseous**

2    **Objects**

3

4    **ABSTRACT**

5    There are three representative planetary formation scenarios: core accretion, pebble accretion and  
6    gravitational disk instability. Most extrasolar gas giant planets discovered to date are thought to stem  
7    from the first, being preferentially observed around metal-rich host stars. Here, I present the 589  
8    samples comprising radial-velocity-observed gas giants and brown-dwarf candidates, in four mass  
9    regimes with boundary values of 5, 15 and 31 Jupiter-mass, in terms of the host-star metallicity. The  
10   larger mass limit is naturally explained as the boundary between planet and binary-star formations.  
11   The three components of gas giants resulting from the middle- and lower-mass boundaries are thought  
12   to represent the dependence of the three planetary formation processes on disk metallicity. Although  
13   gas giants orbiting the metal-rich stars form more easily via core accretion and pebble accretion,  
14   gravitational disk instability is more likely to occur in environments around metal-poor stars.

15

16   **Background**

17   Decades ago, the planetary formation theory<sup>1</sup> was developed for the solar system. Two representative  
18   formation scenarios for Jupiter have been proposed: core accretion<sup>2,3,4</sup> and disk instability<sup>5,6,7</sup> (see  
19   Supplementary Information for details). In theory, the two planetary formation processes have different  
20   dependencies on disk metallicity [Fe/H], which is defined as the ratio of the metal number densities to  
21   hydrogen atoms. Regarding the core accretion scenario, a proto-planet core grows to the critical core  
22   mass more easily as the disk metallicity increases<sup>8,9</sup>, because the disk metallicity reflects the building

23 materials available for the core. In contrast, disk-instability-induced planetary formation tends to occur  
24 for a lower disk metallicity because the cooling time is longer for a higher opacity (related to the disk  
25 metallicity)<sup>10,11</sup>. Note that there also exist reports of no correlation<sup>12</sup> and a very weak positive  
26 correlation<sup>13</sup> between disk metallicity and disk-instability-induced planetary formation in the metallicity  
27 range of the stars hosting the observed planets. Jupiter's envelope has more heavy elements than that of  
28 the Sun<sup>14</sup>; thus, the core accretion scenario is widely accepted as the standard formation process for  
29 Jupiter.

30 Since the first planet orbiting a normal star was discovered in 1995<sup>15</sup>, large-sized radial velocity  
31 observations have revealed that extrasolar gas giants preferentially orbit metal-rich stars<sup>16,17</sup>, and that the  
32 metallicities of stars hosting smaller planets (i.e., Neptune-like planets) are significantly lower than those  
33 of stars orbited by gas giants<sup>18,19</sup>. Because the central star and its surrounding protoplanetary disk are  
34 formed from the same molecular cloud, according to the primordial hypothesis, most gas giants are  
35 thought to have formed via core accretion<sup>8,9</sup>. Direct imaging of extrasolar planets orbiting HR 8799,  
36 Fomalhaut, and Beta Pictoris reported in 2008<sup>20,21</sup> and 2010<sup>22</sup>, respectively, confirmed the existence of  
37 outer planets, which can be explained by the gravitational instability scenario rather than the extended  
38 core accretion scenario with migration or planet–planet scattering<sup>23</sup>. In addition, the extensive planet  
39 searches performed near metal-poor stars<sup>24,25</sup> have revealed a planet fraction of a few percentage points<sup>26</sup>,  
40 which is larger than previously expected. On the other hand, because massive cores in the outer region  
41 beyond 10 AU presumably form through pebble accretion, as proposed recently<sup>27,28</sup>, directly imaged  
42 planets can also be explained by the pebble accretion scenario. Thus, these several planetary formation  
43 processes are possibly the source of the wide variety of planetary systems.

44 Here I explore the possibility of multiple populations in the extrasolar planetary systems discovered to  
45 date. I find that there are four gaseous-object mass regimes based on two-sample Anderson-Darling tests

46 and cluster analysis of gaseous samples in terms of the host-star metallicity distribution. Additionally, I  
47 investigate the physics behind these four groups in terms of the host-star metallicity, considering the  
48 three planetary formation scenarios and the selection effects of the radial-velocity method.

49

## 50 **Multiple components of gaseous objects**

51 I first apply two-sample Anderson–Darling tests<sup>29</sup> to the 589 gaseous samples to examine the relationship  
52 between the metallicity of the central star and the mass of the orbiting object. Since this study aims to  
53 observationally understand the manner in which extrasolar gas giants are formed, low-mass objects such  
54 as Neptune-like planets (gas-dwarf objects), super-Earths, and terrestrial planets, which are thought to  
55 exhibit different formation histories compared to gas giants, are excluded. I apply 0.1 Jupiter-mass as  
56 the lower boundary mass and 0.1 solar-mass as the upper limit (Method section).

57 Figure 1a shows the results of the two-sample Anderson–Darling tests in terms of host-star metallicity  
58 and as a function of the boundary mass, which divides the gaseous object samples into two subsamples.

59 Three inflection points are confirmed: two local p-value minima at 5 and 31 Jupiter-mass and one local  
60 p-value peak at 15 Jupiter-mass. In addition to the two-sample Anderson–Darling test, I apply a cluster

61 analysis to the 589 samples selected as the gaseous objects to investigate how many components they  
62 contain. This analysis is conducted according to a method proposed in a previous study<sup>30</sup>. Figure 2 shows

63 the host-star metallicity and companion mass distributions for four- and five-component models selected  
64 by the cluster analysis. The difference between these models is the existence or non-existence of the

65 lowest mass boundary of 1 Jupiter-mass. Note that the cluster analysis for all 722 samples also supports  
66 the four-component model of gaseous objects, and the boundary between the gaseous objects and the

67 gas-dwarf objects is consistent with 0.1 Jupiter-mass (Extended Data Figure 1). The three masses at the  
68 inflection points in the results of the two-sample Anderson–Darling test are almost consistent with the

69 three boundaries except for the boundary of 1 Jupiter-mass derived by cluster analysis. Based on these  
70 considerations, the four-component model is selected as the best suited model for gaseous objects. Note  
71 that, because the density of the lowest mass group (grey dots in Figure 2a) is much less than that of the  
72 second lowest group (green dots in Figure 2a), the lowest mass samples possibly experience a halt of the  
73 rapid gas accretion onto the core and/or are partially affected by the selection effects of radial velocity  
74 observations.

75 Next, I derive the average metallicities according to the four-component model of the gaseous samples  
76 (Method section). Figure 1b shows the average metallicities of the host stars for five subsamples  
77 separated by the three boundary masses in the two-sample Anderson–Darling test. Gaseous samples  
78 lighter than 5 Jupiter-mass and low-mass brown dwarfs with masses ranging from 15 to 31 Jupiter-mass  
79 preferentially orbit metal-rich stars, but massive gas giants with masses ranging from 5 to 15 Jupiter-  
80 mass weakly depend on the host-star metallicity. In addition, the average metallicity of massive brown-  
81 dwarf candidates with masses exceeding 31 Jupiter-mass is significantly lower than those of the other  
82 three subsamples, and is consistent with that of the High Accuracy Radial Planet Searcher (HARPS)  
83 program<sup>31</sup>. Since the fraction of the brown dwarfs more massive than 31 Jupiter-mass is independent of  
84 the metallicity, the largest boundary mass is thought to represent the upper limit for objects formed via  
85 core accretion. In fact, the upper limit is almost consistent with the findings from the previous theoretical  
86 calculations<sup>33,34</sup>.

87 I redefine the samples lighter than 31 Jupiter-mass as planetary-mass objects from the standpoint of  
88 planetary formation and label the samples with masses ranging from 0.1 to 5 Jupiter-mass as  
89 ‘intermediate-mass planets’. In addition, two subsamples with masses from 5 to 15 Jupiter-mass and  
90 from 15 to 31 Jupiter-mass are labeled as ‘massive planets’ and ‘very massive planets’, respectively.  
91 Note that the boundary between planetary mass and brown dwarf objects established by the deuterium-

burning minimum mass<sup>35</sup> of  $\sim 10$  Jupiter-mass mentioned in a previous study is semantic<sup>36</sup>; this value has no physical meaning from the perspective of object evolution.

## Two planet deserts

I now discuss the cause behind grouping the 589 gaseous objects into groups defined by four components. The four-component model results from relative paucity of the samples in two specific regions in the diagram of host-star metallicity versus companion mass; the two regions indicate very massive planets ( $15 \leq M_p < 31M_J$ ) and intermediate-mass planets ( $0.1 \leq M_p < 5M_J$ ) around low-metallicity stars ( $[\text{Fe}/\text{H}] \leq -0.2$ ). In other words, the mass distribution of the gaseous samples orbiting metal-poor stars differs from that around non-metal-poor stars. However, all samples selected for this study, which are detected via radial velocity observations to retain sample homogeneity, are generally influenced by two selection effects<sup>37, 38</sup>: (i) limited sensitivity to long-period planets owing to short observation terms and (ii) limited sensitivity to low-mass planets owing to a lack of measurement precision in radial velocity observations. In this section, I examine whether the planetary mass distribution around metal-poor stars is produced by these selection effects.

Based on the same criteria, I first select two gaseous subsamples: one subsample orbiting metal-poor stars ( $[\text{Fe}/\text{H}] \leq -0.2$ ) and the other orbiting stars with metallicities higher than solar-metallicity ( $[\text{Fe}/\text{H}] \geq 0$ ). This approach is used because the selection effects influence the subsamples for the metal-poor stars and the non-metal-poor stars. This evaluation extracts the samples that are not strongly influenced by the selection effects of the radial velocity observations around metal-poor stars<sup>38</sup> (see Method section). Figures 3a and 3b show the distributions of the semi-major axes and the companion

masses for the two extracted subsamples, categorized according to the host-star metallicity, respectively.

Two main groups appear around the stars with metallicity higher than solar-metallicity: short-period

115 intermediate-mass planets (i.e. hot Jupiters) and long-period intermediate-mass planets. Planets not in  
116 the two groups are sparsely distributed. In contrast, the metal-poor samples are not continuously  
117 distributed and are clustered into three groups: long-period intermediate-mass planets, long-period  
118 massive planets and long-period brown-dwarf candidates with masses exceeding 31 Jupiter-mass. The  
119 lack of very massive planets around the metal-poor samples is confirmed in the region where the samples  
120 are not strongly influenced by the selection effect.

121 Next, I evaluate planet mass distributions in the two extracted subsamples. Figure 3c shows the  
122 cumulative mass distributions of the two extracted subsamples orbiting the metal- and non-metal-poor  
123 stars. Of the extracted samples orbiting the stars with metallicities higher than solar-metallicity (black  
124 dots in Figure 3a), approximately 80% are categorized as intermediate-mass planets. In contrast, more  
125 than half of the extracted samples associated with the metal-poor stars (black dots in Figure 3b) have  
126 masses greater than 5 Jupiter-mass. In other words, the fraction of massive planets to intermediate-mass  
127 around metal-poor stars is much larger than that around the non-metal-poor stars, which confirms the  
128 lack of intermediate-mass planets relative to massive planets around metal-poor stars. Thus, the multiple  
129 populations of extrasolar gaseous objects reflect a difference in their planetary formation processes.

130

### 131 **Beyond the standard core accretion model**

132 I now discuss whether the relationship between host-star metallicity and companion mass is naturally  
133 explained by the current planet formation models. To begin, I examine how the core accretion mechanism  
134 is responsible for the multiple components of gaseous objects. As revealed in previous studies<sup>16,17</sup>, there  
135 is a strong correlation between planet fraction and host-star metallicity. From the perspective of core  
136 accretion theory, this behavior occurs because the core more easily reaches a critical core mass<sup>3</sup> if the  
137 disk metallicity is higher. A critical disk metallicity exists, which enables a given core to reach the critical

138 core mass before disk depletion occurs<sup>39</sup>. As discussed in the Supplementary Information, the critical  
139 disk metallicities are estimated to be  $-0.4$  and  $-0.9$  dex for gas surface densities of 3 and 10 times the  
140 Minimum Mass Solar Nebulae (MMSN) model value<sup>40</sup>, respectively, under a certain assumption<sup>41,42</sup>. On  
141 the other hand, the final mass of a core-accreted planet is also thought to depend on the disk metallicity  
142 because the runaway gas accretion onto the core begins at an earlier stage as a result of the higher disk  
143 metallicity<sup>9</sup>. Because the very massive planets preferentially orbit metal-rich stars (Figures 1 and 2),  
144 another critical metallicity actually exists that allows gaseous proto-planets to grow to a disk mass. In  
145 addition, focusing on the fact that the distribution of the brown-dwarf candidates with masses exceeding  
146 31 Jupiter-mass are independent of the host-star metallicities (Figures 1 and 2), I expect that the very  
147 massive planets are consistent with the upper mass limit of core-accreted planets. Thus, planetary mass  
148 objects with masses ranging from 0.1 to 31 Jupiter-mass around solar-metallicity and metal-rich stars are  
149 naturally explained by the core accretion scenario. The mass distribution of planets orbiting solar-  
150 metallicity and metal-rich stars is also consistent with the prediction<sup>33</sup> from the core accretion theory.  
  
151 Another possibility exists for the formation of massive and very massive planets around metal-rich stars.  
152 As shown in Figure 3, massive and very massive planets are located in the outer region. While the  
153 timescale for core growth to the critical core mass is longer via the standard core-accretion for larger  
154 semi-major axes, pebble accretion shortens this timescale for core growth in the outer region (see  
155 Supplementary Information). If pebble accretion effectively works for core formation, the upper mass  
156 limit of planets formed via pebble accretion is expected to increase for greater disk metallicity in the  
157 same manner as that for the standard core accretion model. This result is due to the enhanced accretion  
158 rate of pebbles onto a core enhances for higher disk metallicity<sup>43</sup>, and at an earlier stage, massive cores  
159 can be easily formed in regions farther out<sup>44</sup>. Thus, the result of observations for the solar-metallicity  
160 and metal-rich samples is also supported by the pebble accretion scenario.

161 In contrast, the excess of massive planets orbiting metal-poor stars differs from that expected from the  
162 core accretion formation theory. The semi-major axes of the massive samples orbiting metal-poor stars  
163 also differ from those around metal-rich stars (Figure 3). Here, I describe why the observed masses and  
164 orbital properties around metal-poor stars cannot be explained by the standard core accretion and pebble  
165 accretion models: the so-called ‘bottom-up’ models. The excess of massive planets orbiting metal-poor  
166 stars is unlikely in the bottom-up scenarios because the timescale of planet growth is longer for larger  
167 planetary masses; therefore, a continuous decrease in the planetary mass function is predicted<sup>33</sup> (see also  
168 Supplementary Information). In addition, although proto-gaseous planets tend to obtain more mass in  
169 the outer region<sup>45,46</sup>, the semi-major axes of massive planets around metal-poor stars are locally  
170 distributed from 0.5 to 2 AU (Figure 3b), which are smaller than those around metal-rich stars despite  
171 slower type-II migration around the lower metallicity disks<sup>47</sup>. Therefore, the final masses of planets  
172 orbiting metal-poor stars are expected to be lighter than those around metal-rich stars. Additionally, while  
173 the eccentricities of massive planets embedded in the disk gas tend to be enhanced through the planet-  
174 disk interaction prior to gas dissipation<sup>48</sup>, the eccentricities of planets orbiting metal-poor stars are locally  
175 distributed from 0.1 to 0.3 (Extended Data Figure 2b). Conversely, the eccentricity distribution around  
176 metal-rich stars is naturally explained by the extended standard core accretion model.

177 An explanation for the excess massive planets orbiting metal-poor stars is that the disk instability acts in  
178 the vicinity of metal-poor stars, because a lower mass limit applies for planets formed via the disk  
179 instability mechanism (i.e. corresponding to an order of the Jeans mass<sup>39,49</sup>). As a result, a sharp increase  
180 appears in the planetary mass function at 5 Jupiter-mass. If an upper limit of the planets formed via disk  
181 instability actually exists (see Supplementary Information), the lack of the very massive planets around  
182 metal-poor stars can be explained. In addition, it is accepted that planet formation due to disk instability  
183 tends to occur in the vicinity of metal-poor stars because the cooling timescale in the disk mid-plane is

184 reduced due to low disk opacity<sup>10,11</sup>. The low eccentricities of the massive planets are also consistent  
185 with numerical simulations<sup>49,50</sup> and the eccentricities of HR 8799 bcde<sup>51</sup>. Note that the four planets  
186 orbiting HR 8799 are located in a region beyond the standard core-accretion model in Figure 4 (i.e., they  
187 are the candidates for disk instability planets); therefore, this categorization is supported by a previous  
188 theoretical expectation<sup>23</sup>. However, there is a controversial point regarding the disk instability hypothesis.  
189 Although planets formed via disk instability tend to appear at a distance of a few AUs from the host star,  
190 as shown in several simulations<sup>6,7,49,50,52</sup>, most of the planets discovered around metal-poor stars are  
191 distributed from 0.5 to 3 AU (Figure 3b). Whether disk-instability-formed planets migrate to a distance  
192 of a few AUs from the host star after their formation in the outer disk remains an open question.

193

## 194 Discussion

195 I compare the distribution of the host-star metallicities and the planetary masses for all 722 samples  
196 compiled in Extended Data Table 2 with the distribution expected from the three planetary formation  
197 theories (Figure 4). Two scarce regions appear in terms of object mass, one at 0.1–0.5 Jupiter-mass and  
198 one at 30–40 Jupiter-mass. Whereas the former arises from the rapid gas accretion onto the core, the  
199 latter represents a gap between binary star and planet formation. In other words, the first and second  
200 regions, respectively, reflect the lower and upper limits on the masses of gaseous objects that are formed  
201 by the planetary formation processes. In addition to the two scarce regions, two planet deserts are also  
202 observed in the host-star metallicity and the planetary mass diagram: (1) intermediate-mass planets and  
203 (2) very massive planets with masses ranging from 15 to 31 Jupiter-mass orbiting metal-poor stars. The  
204 latter desert is thought to result from the critical metallicity for the final mass of objects formed via the  
205 bottom-up mechanisms and the existence of the upper mass limit of planets formed via gravitational disk  
206 instability. The excess of massive planets located between the two scarce regions reflects planet

207 formation via gravitational disk instability. Because these observational results were obtained from the  
208 nearby planetary systems that have been discovered to date, further radial velocity observations are  
209 important for understanding the question of whether multiple populations of extrasolar gas giants exist  
210 truly and universally. If multiple populations of extrasolar gas giants are confirmed in further  
211 observations, the newly discovered population poses the essential question of how the planets belonging  
212 to the new population were formed and evolved.

213 Finally, I discuss the uncertainty of orbital inclination,  $i$ , associated with the lower limit of companion  
214 mass. All the samples constructed for this study are detected by radial velocity observations, and the  
215 lower limits of the companion masses,  $M_p \sin i$ , estimated from the radial-velocity observation are used  
216 for the statistical analysis. The model and its parameters derived through the two-sample Anderson–  
217 Darling test considering the indefiniteness of the orbital inclination are shown in Extended Data Figure  
218 3. The three boundary masses are 6.6, 18.6, and 35.3 Jupiter-mass, corresponding to about  $4/\pi$  times the  
219 original boundaries shown in Figure 1. The  $4/\pi$  represents inverse number of the mean  $\sin i$  averaged  
220 over all solid angle. Thus, the true three boundary masses considering the uncertainty of orbital  
221 inclination are slightly higher than those derived by the Anderson–Darling test using the lower limit of  
222 companion masses.

223

## 224 Methods

### 225 Sample construction

226 The samples considered in this paper are limited to companion objects detected by radial velocity  
227 observations, allowing the orbital parameters to be characterized and the lower limit of the companion  
228 mass to be determined. Essentially, samples are selected from those labeled “Radial Velocity” in the  
229 “detection method” column of the Extrasolar Planet Encyclopedia catalogue<sup>53</sup> as of the end of January

230 2017. Considering the possibility that objects formed through the core accretion process grow to brown-  
231 dwarf-mass levels, the masses of the samples range up to 0.1 solar-mass, corresponding to approximately  
232 ten times that of the MMSN model value<sup>40</sup>, which is nearly the upper limit of the disk mass<sup>41</sup>. Note that  
233 the brown-dwarf candidates discovered via radial velocity observations<sup>54-62</sup> have also been added to this  
234 catalogue. Even though the object masses of some samples are constrained by additional astrometry or  
235 transit observations, I used the lower limit of the object mass,  $M_p \sin i$ , including the indefiniteness of  $i$ ,  
236 the angle of the orbital plane relative to the plane perpendicular to the line-of-sight of the planetary  
237 system, and  $M_p$ , which is the true object mass. This approach is used to retain homogeneity in the object  
238 masses. The number of samples considered in this study is 722. The host-star metallicity, host-star mass  
239  $M_*$ , effective temperature and its reference<sup>97-346</sup> for each host star are compiled in Extended Data Table  
240 1. I refer to the SWEET-Cat catalogue<sup>63</sup> for the metallicity, mass, and effective temperature values of the  
241 host star; this catalogue presents the uniformly derived stellar parameters of planet host stars. To  
242 minimize measurement biases for host-star metallicities, which are not derived using the uniform  
243 method<sup>64,65</sup>, I additionally calibrated these values by using two regression lines determined from the  
244 correlation between the metallicities listed in publications that reported planet detections and those  
245 derived using the uniform method. Note that, because the observed metallicity depends on the effective  
246 temperature of the host star<sup>66</sup>, I divided the samples into two according to the effective temperature of  
247 the host star and derived the two regression lines for hot ( $T_* > 5000K$ ) and cool ( $T_* < 5000K$ ) stars  
248 (Extended Data Figures 4a and 4b), respectively. For some of the brown-dwarf candidates that are not  
249 listed in the SWEET-Cat catalogue, I applied the metallicities measured by the Geneva–Copenhagen  
250 observations<sup>67</sup> and then corrected these values using regression coefficients derived in the same way as  
251 the above calibration. Note that the metallicities listed in the Extrasolar Planet Encyclopedia and the  
252 Geneva-Copenhagen catalogues have good correlations with those derived using the uniform method, as

253 reported in previous studies<sup>31</sup> (Extended Data Figure 4c). The planet name, semi-amplitude of radial  
254 velocity  $K$ , orbital period  $P$ , eccentricity  $e$ , lower limit of object mass  $M_p \sin i$ , semi-major axis  $a$  and  
255 its reference<sup>97-346</sup>, for each companion are compiled in Extended Data Table 2. Of these,  $M_p \sin i$  and  $a$   
256 are calculated using the following equation<sup>68</sup> and Kepler's Third Law, respectively, because the host-star  
257 masses listed in Extended Data Table 1 are revised:

$$258 M_p \sin i = 4.919 \times 10^{-3} \left( \frac{K}{m/s} \right) \sqrt{(1 - e^2)} \left( \frac{P}{1 day} \right)^{1/3} \left( \frac{M_*}{M_\odot} \right)^{2/3} M_J, \quad (1)$$

259 where  $M_\odot$  and  $M_J$  represent the solar-mass and Jupiter-mass, respectively.

260

## 261 Selection of gaseous objects

262 The gaseous objects from all the samples used in this study are extracted in order to remove the impact  
263 of low-mass samples, such as Neptune-mass planets (gas dwarfs) and super-Earths, on the two-sample  
264 Anderson–Darling tests and the cluster analysis. First, I determined the boundary mass between the  
265 gaseous and gas-dwarf objects from a perspective of both theory and observation. Because the masses  
266 of the gaseous objects and gas dwarfs may overlap, the gaseous samples used for the Anderson–Darling  
267 tests were selected by excluding items lighter than gas dwarfs. According to a previous study<sup>45</sup>, gas-  
268 dwarf objects, which primarily consist of heavy-core objects such as Neptune and Uranus, have the  
269 potential to grow to the extent allowed by the core building materials inside their orbital semi-major axes.  
270 This growth occurs via giant impacts in the inner region of the disk after the disk gas dissipates. However,  
271 the core growth is limited by the scattering effect of the heavy core, which increases with greater  
272 distances from the central star. Therefore, the mass of a gas-dwarf object reaches a maximum at the  
273 semi-major axis, where the scattering effect begins to limit the core growth. Given that the ratio of the  
274 collision-to-ejection probabilities for the heavy core is 0.1 and the core density is 1 g/cm<sup>3</sup>, the upper-

275 limit on the mass of a gas-dwarf object,  $M_{gd,max}$ , is

276

$$M_{gd,max} \simeq 0.37 M_J \left( \frac{\eta_{ice}}{4} \right)^{3/4} \left( \frac{f_d}{10} \right)^{3/4}, \quad (2)$$

277 where  $\eta_{ice}$  is the dust surface-density enhancement factor due to ice condensation and  $f_d$  is the scaling  
278 factor of the dust surface density relative to the MMSN model value. Considering a factor of the solid-  
279 angle average of  $\sin i / \pi/4$ , the upper mass limits on a gas-dwarf object are estimated to be  
280 approximately 0.1 and 0.3 Jupiter-mass for dust surface densities of 3 and 10 times the MMSN model  
281 value, respectively. On the other hand, a boundary between the gas giants and the gas dwarfs at four  
282 times the Earth's radius has been observationally revealed by the Kepler data<sup>69</sup>. I found that the mass  
283 corresponding to the boundary is consistent with the above theoretical estimation for 3 times the MMSN  
284 model value, obtained using the empirical planetary mass–radius relation for a planetary mass of less  
285 than 150 times the Earth's mass<sup>70</sup>, where the time-averaged incident flux of the planet is set to  $10^8$   
286 erg/s/cm<sup>2</sup>, corresponding to the flux of a typical non-hot Jupiter. Based on these considerations, 0.1

287 Jupiter-mass is applied in this study as the boundary mass between the gas giants and the gas dwarfs.

288 The boundary value of 0.1 Jupiter mass is also highly consistent with the result of the cluster analysis

289 (Extended Data Figure 1).

290 In contrast, the upper limit on the masses of the gaseous objects formed via the planetary formation  
291 processes is not yet well understood, either theoretically or observationally, owing to the limited  
292 observational results for brown-dwarf objects. Therefore, I set an upper limit on the sample masses of  
293 0.1 solar-mass, corresponding to 10 times the MMSN model (maximum disk-mass value). Note that, as  
294 the number of brown-dwarf candidates used in this study is small, the upper limit on the sample masses  
295 does not affect the two-sample Anderson–Darling tests or the cluster analysis.

296

297

298      **Two-sample Anderson–Darling test**

299      I now explain the procedure to obtain the results shown in Figure 1a of the two-sample Anderson–Darling  
 300     test. The (two-sample) Anderson–Darling test<sup>29</sup> is categorized as a non-parametric test that can be  
 301     applied to any probability density function(s). The Anderson–Darling test has several advantages over  
 302     the Kolmogorov-Smirnov test<sup>71</sup>. The procedure is as follows. I first divide the gaseous samples into two  
 303     subsamples based on a boundary mass  $M_b$  that ranges from the lower to the upper limits of the sample  
 304     masses. Next, I define a test statistic denoted as AD in the two-sample Anderson–Darling test, such that

$$305 \quad \text{AD} = \frac{1}{mn} \sum_{i=1}^{n+m} \frac{(M_i Z_{(n+m-i)})^2}{i Z_{(n+m-i)}}, \quad (3)$$

306     where  $n$  and  $m$  indicate the two sample sizes  $X_{(n)}$  and  $Y_{(m)}$ , and  $Z_{(n+m)}$  indicates the samples  
 307     constructed by summing the two samples  $X_{(n)}$  and  $Y_{(m)}$  and ordering the combined samples.  $N_i$  is the  
 308     number of observations in one of the two samples,  $X_{(n)}$ , that are equal to or less than observation  $i$  in the  
 309     combined samples  $Z_{(n+m)}$ . I calculate  $P$ -values, to indicate the statistical significance of the difference  
 310     between the two empirical distributions. The  $P$ -value is defined as

$$311 \quad P = 1 - Pr(AD \leq Z), \quad (4)$$

312     where  $Pr(AD \leq Z)$  is the probability that the AD value is less than a statistical value  $Z$ . As the  $P$ -value  
 313     decreases, the statistical significance increases. For a larger number of items in the two subsamples, the  
 314     probability follows the limiting distribution of the Anderson–Darling test<sup>72</sup>.

$$315 \quad Pr(AD \leq Z) = \sqrt{\frac{\pi}{2}} \frac{1}{z} \sum_{j=0}^{\infty} \frac{(-1)^j \Gamma(j + \frac{1}{2})}{\Gamma(\frac{1}{2}j)!} \int_0^1 \frac{4j+1}{\sqrt{r^3(1-r)}} \exp\left(\frac{rz}{8} - \frac{\pi^2(4j+1)^2}{8rz}\right) dr, \quad (5)$$

316     where  $j$  is a positive integer and  $\Gamma$  is the Gamma function. Given that the measurement errors follows a  
 317     normal distribution, I sample the host-star metallicities and planet masses. Based on the above equations,  
 318     I finally derive the  $P$ -values, changing the boundary planet mass from 0.3 to  $60 M_J$  in steps of  $0.05 M_J$ .  
 319     Based on the method described in a previous study<sup>30</sup>, I repeat this process 100000 times. After this

320 iteration, I average the calculated  $P$ -values for each divided point and derive the standard deviation of  
321 the  $P$ -values. As shown in Figure 1a, the  $P$ -values are given as a function of  $M_b$ , which corresponds to  
322 the horizontal axis in Figure 1a. Thus, I can quantitatively evaluate the statistically significant difference  
323 between the probability distributions for two samples with the  $P$ -value calculated via the two-sample  
324 Anderson–Darling test.

325

### 326 Selection of model and derivation of parameters for gaseous objects

327 The 589 gaseous objects are divided into four mass regimes in terms of the host-star metallicities based  
328 on the two-sample Anderson–Darling tests and the cluster analysis. The parameters of the selected model  
329 are estimated as shown in Figure 1b. To avoid the multiple comparisons problem that leads to an incorrect  
330 uncertainty in statistical inference, the following procedure is applied according to a previous study<sup>30</sup>:  
331 first, I sample the host-star metallicities and the planet masses, provided that these measurement errors  
332 follow a normal distribution. I divide the samples randomly into two groups in half and search for two  
333 local  $P$ -value minima and one local  $P$ -value peak with the two-sample Anderson–Darling test in the first  
334 half sample. Note that the two  $P$ -value minima are identified in the two mass regions  $M_p \leq 10M_J$  and  
335  $20M_J < M_p$  and the one local  $P$ -value peak is identified in the mass region  $10 < M_p \leq 20M_J$ . I estimate  
336 the mean metallicities for the four groups that are divided by the two planet masses at the local  $P$ -value  
337 minimum and the one planet mass at the local  $P$ -value peak. I iterate the calculation over 100000 times.  
338 Figure 1b shows the resulting mean metallicities and standard deviations for the four mass regions.

339

### 340 Cluster analysis

341 Cluster analysis<sup>73</sup> is conducted to investigate how many components may be identified in the extrasolar  
342 gaseous objects. The best suited model for the gaseous samples is identified as follows: the *mclust*

343 package<sup>74</sup> in *R* is used to fit two-dimensional Gaussian mixture models to the diagram of the host-star  
344 metallicities versus the companion masses. The number of components of the Gaussian mixture models  
345 used for this cluster analysis ranges from 1 to 8. I first sample the host-star metallicities and companion  
346 masses given that the measurement errors follow a normal distribution. Next, I determine the number of  
347 components of the best Gaussian mixture model based on the Bayesian Information Criterion<sup>75</sup> and check  
348 to which component each sample belongs. I repeat this procedure 10000 times. Figure 2 and Extended  
349 Data Figure 1 show the best Gaussian mixture models for the 589 gaseous objects and all 722 samples,  
350 respectively.

## 352 Evaluation of selection effects

353 To remove the dependency of the selection effects on host-star metallicity, two subsamples are extracted  
354 from the two samples orbiting metal- and non-metal-poor stars with the same criteria, respectively. I  
355 define samples, which can be detected by half of the radial velocity observations that discovered  
356 companions around metal-poor stars, as non-biased samples. I thus obtain the mass distributions for the  
357 two non-biased samples categorized according to the host-star metallicity. The non-biased samples have  
358 to satisfy the following criteria:

- 359 1. The semi-velocity amplitude of a star hosting a non-biased sample is greater than accuracy  
360 corresponding to a 99% detection rate of radial velocity observation.
- 361 2. The orbital period of a non-biased sample is shorter than the observational term.

362 The velocity amplitude required for achieving the 99% detection rate,  $K_{99}$ , is calculated using<sup>38</sup>

$$363 K_{99} \approx 10.2\sqrt{N} \left( \frac{\sigma}{1m/s} \right) m/s, \quad (6)$$

364 where  $N$  is the number of measurements and  $\sigma$  is the quadratic sum of radial velocity measurement error  
365 and stellar jitter. The majority of radial velocity errors larger than 10 m/s are not limited by the

366 instrumental accuracy but rather by stellar jitter, which depends on the spectral type and luminosity class  
367 of a star<sup>76-78</sup>. Note that, although the above equation was originally derived for a single planetary system,  
368 the detectability for multiple planetary systems can also be applied when the number of measurements  
369 exceeds 20. Because the numbers of measurements for most of the radial velocity observations compiled  
370 in Extended Data Table 3 exceed 20, I assume only a small impact on the detection rates of the multiple  
371 planetary systems.

372 Based on these considerations, I extract the two non-biased samples orbiting metal- and non-metal-poor  
373 stars, and then derive the cumulative mass distributions for the two non-biased samples. I iterate the  
374 procedure over 100000 times in the calculation to reflect the measurement errors of semi-velocity  
375 amplitude, orbital period, and host-star metallicity. The black dots in Figure 3 and Extended Data Figure  
376 2 indicate the samples that are detected by more than half the radial velocity observations around metal-  
377 poor samples on average through the 100000 iterations. Note that the parameters of the radial velocity  
378 observations around metal-poor stars are compiled in Extended Data Table 3.

379

## 380 References

- 381 1. Hayashi, C. Nakazawa, K. & Nakagawa, Y. Formation of the solar system. *Protostars and Planets II*.  
382 Tucson AZ, University of Arizona Press 1100-1153 (1985).
- 383 2. Perri, F. & Cameron, A. G. W. Hydrodynamic instability of the solar nebula in the presence of a  
384 planetary core. *Icarus* **22**, 416-425 (1974).
- 385 3. Mizuno, H. Formation of the giant planets. *Prog. Theor. Phys.* **64**, 544-577 (1980).
- 386 4. Pollack, J. B. *et al.* Formation of the giant planets by concurrent accretion of solids and gas. *Icarus*  
387 **124**, 62-85 (1996).

- 388 5. Kuiper, G. P. On the origin of the solar system. *Proc. Nat. Aca. Sci.* **37**, 1-14 (1951).
- 389 6. Boss, A. P. Giant planet formation by gravitational instability. *Science* **276**, 1836-1839 (1997).
- 390 7. Mayer, L. Quinn, T. Wadsley, J. & Stadel, J. Formation of Giant Planets by Fragmentation of  
391 Protoplanetary Disks. *Science* **298**, 1756-1759 (2002).
- 392 8. Ida, S. & Lin, D. N. C. Toward a deterministic model of planetary formation. II. The formation and  
393 retention of gas giant planets around stars with a range of metallicities. *Astrophys. J.* **616**, 567-572  
394 (2004).
- 395 9. Mordasini, C. Alibert, Y., Benz, W., Klahr, H. & Henning, T. Extrasolar planet population synthesis.  
396 IV. Correlations with disk metallicity, mass, and lifetime. *Astron. Astrophys.* **541**, A97 (2012).
- 397 10. Cai, K. *et al.* The effects of metallicity and grain size on gravitational instabilities in protoplanetary  
398 disks. *Astrophys. J.* **636**, 149-152 (2006).
- 399 11. Durisen, R. H. *et al.* Gravitational instabilities in gaseous protoplanetary disks and implications for  
400 giant planet formation. *Protostars and Planets V*, Reipurth, V. Jewitt, D. and Keil, K. (eds.), Univ.  
401 of Arizona Press, Tucson **951**, 607-622 (2007).
- 402 12. Boss, A. P. Stellar metallicity and the formation of extrasolar gas giant planets. *Astrophys. J.* **567**,  
403 149-153 (2002).
- 404 13. Mayer, L. Lufkin, G. Quinn, T. & Wadsley, J. Fragmentation of gravitationally unstable gaseous  
405 protoplanetary disks with radiative transfer. *Astrophys. J.* **661**, 77-80 (2007).
- 406 14. Young, R. E. The Galileo probe: how it has changed our understanding of Jupiter. *New Astron. Rev.*  
407 **47**, 1-51 (2003).
- 408 15. Mayor, M. & Queloz, D. A Jupiter-mass companion to a solar-type star. *Nature* **378**, 355-359 (1995).

- 409 16. Santos, N. C. Israelián, G. Mayor, M., Rebolo, R. & Udry, S. Statistical properties of exoplanets. II.
- 410 Metallicity, orbital parameters, and space velocities. *Astron. Astrophys.* **398**, 363-376 (2003).
- 411 17. Fischer, D. A. & Valenti, J. The planet-metallicity correlation. *Astrophys. J.* **622**, 1102-1117 (2005).
- 412 18. Mayor, M. *et al.* The HARPS search for southern extra-solar planets XXXIV. Occurrence, mass
- 413 distribution and orbital properties of super-Earths and Neptune-mass planets. Preprint at
- 414 <https://arxiv.org/abs/1109.2497>.
- 415 19. Wang, J. & Fischer, D. A. Revealing a universal planet-metallicity correlation for planets of different
- 416 sizes around solar-type stars. *Astron. J.* **149**, 14 (2015).
- 417 20. Marois, C. *et al.* Direct imaging of multiple planets orbiting the star HR 8799. *Science* **322**, 1348-
- 418 1352 (2008).
- 419 21. Kalas, P. *et al.* Optical images of an exosolar planet 25 light-year from Earth. *Science* **322**, 1345-
- 420 1348 (2008).
- 421 22. Lagrange, A.-M. *et al.* A giant planet imaged in the disk of the young star  $\beta$  pictoris. *Science* **5987**,
- 422 57-59 (2010).
- 423 23. Dodson-Robinson, S. E., Veras, D., Ford, E. B. & Beichman, C. A. The formation mechanism of gas
- 424 giants on wide orbits. *Astrophys. J.* **707**, 79-88 (2009).
- 425 24. Sozzetti, A. *et al.* A Keck HIRES Doppler search for planets orbiting metal-poor dwarfs. II. On the
- 426 frequency of giant planets in the metal-poor regime. *Astrophys. J.* **697**, 544-556 (2009).
- 427 25. Santos, N. C. *et al.* The HARPS search for southern extrasolar planets. XXV. Results from the metal-
- 428 poor sample. *Astron. Astrophys.* **526**, 112 (2011).
- 429 26. Mortier, A. *et al.* The frequency of giant planets around metal-poor stars. *Astron. Astrophys.* **543**,

- 430 A45 (2012).
- 431 27. Ormel, C. W. & Klahr, H. H. The effect of gas drag on the growth of protoplanets. Analytical  
432 expressions for the accretion of small bodies in laminar disks. *Astron. Astrophys.* **520**, A43 (2010).
- 433 28. Lambrechts, M. & Johansen, A. Rapid growth of gas-giant cores by pebble accretion. *Astron.*  
434 *Astrophys.* **544**, A32 (2012).
- 435 29. Pettitt, A. N. A two-sample Anderson–Darling rank statistic. *Biometrika* **63**, 161 (1976).
- 436 30. Schlaufman, K. C. A continuum of Planet Formation Between 1 and 4 Earth Radii. *Astrophys. J.* **799**,  
437 L26 (2015).
- 438 31. Sousa, S. G., Santos, N. C., Israelian, G., Mayor, M. & Udry, S. Spectroscopic stellar parameters for  
439 582 FGK stars in the HARPS volume-limited sample. Revising the metallicity-planet correlation.  
440 *Astron. Astrophys.* **533**, A141 (2011b).
- 441 32. Valenti, J. A. & Fisher, D. A. Spectroscopic properties of cool stars (SPOCS). I. 1040 F, G, and K  
442 dwarfs from Keck, Lick, and AAT Planet Search Programs. *Astrophys. J. Suppl.* **159**, 141-166 (2005).
- 443 33. Mordasini, C. Alibert, Y. Benz, W. & Naef, D. Extrasolar planet population synthesis. II. Statistical  
444 comparison with observations. *Astron. Astrophys.* **501**, 1161-1184 (2009).
- 445 34. Tanigawa, T. & Tanaka, H. Final masses of giant planets II. Jupiter formation in a gas-depleted disk.  
446 *Astrophys. J.* **823**, 48 (2016).
- 447 35. Chabrier, G. & Baraffe, I. Theory of low-mass stars and substellar objects. *Ann. Rev. Astron.*  
448 *Astrophys.* **38**, 337-377 (2000).
- 449 36. Chabrier, G., Johansen, A., Janson, M., & Rafikov, R. Giant planet and brown dwarf formation.  
450 *Protostars and Planets IV*. by Beuther, H. Klessen, R. S. Dullemond, C. P. & Henning, T. (eds.)

- 451 Tucson AZ, University of Arizona Press **914**, 619-642 (2014).
- 452 37. Nelson, A. F. & Angel, J. R. P. The range of masses and periods explored by radial velocity searches  
453 for planetary companions. *Astrophys. J.* **500**, 940-957 (1998).
- 454 38. Narayan, R. Cumming, A. & Lin, D. N. C. Radial velocity detectability of low-mass extrasolar  
455 planets in close orbits. *Astrophys. J.* **620**, 1002-1009 (2005).
- 456 39. Matsuo, T. Shibai, H. Ootsubo, T. & Tamura, M. Planetary formation scenarios revisited: Core-  
457 accretion versus disk instability. *Astrophys. J.* **662**, 1282-1292 (2007).
- 458 40. Hayashi, C. Structure of the solar nebula, growth and decay of magnetic fields and effects of magnetic  
459 and turbulent viscosities on the nebula. *Prog. Theor. Phys. Suppl.* **70**, 35-53 (1981).
- 460 41. Williams, J. P. & Cieza, L. A. Protoplanetary Disks and Their Evolution. *Ann. Rev. Astron. Astrophys.*  
461 **49**, 67-117 (2011).
- 462 42. Wyatt, M. C. Dent, W. R. F. & Greaves, J. S. SCUBA observations of dust around Lindroos stars:  
463 evidence for a substantial submillimetre disc population. *Mon. Not. Roy. Astron. Soc.* **342**, 876-888  
464 (2003).
- 465 43. Lambrechts, M. & Johansen, A. Forming the cores of giant planets from the radial pebble flux in  
466 protoplanetary discs. *Astron. Astrophys.* **572**, A107 (2014).
- 467 44. Bitsch, B. Lambrechts, M. & Johansen, A. The growth of planets by pebble accretion in evolving  
468 protoplanetary discs. *Astron. Astrophys.* **582**, A112 (2015).
- 469 45. Ida, S. & Lin, D. N. C. Toward a deterministic model of planetary formation. I. A desert in the mass  
470 and semi-major axis distributions of extrasolar planets. *Astrophys. J.* **604**, 388-413 (2004).
- 471 46. Mordasini, C. Alibert, Y. & Benz, W. Extrasolar planet population synthesis. I. Method, formation

- 472 tracks, and mass-distance distribution. *Astron. Astrophys.* **501**, 1139-1160 (2009).
- 473 47. Livio, M. & Pringle, J. E. Metallicity, planetary formation and migration. *Mon. Not. Roy. Astron.*  
474 *Soc.* **346**, 42-46 (2003).
- 475 48. Kley, W. & Dirksen, G. Disk eccentricity and embedded planets. *Astron. Astrophys.* **447**, 369-377  
476 (2006).
- 477 49. Mayer, L. Formation via Disk Instability. *Formation and Evolution of Exoplanets*, by Barns, R. (eds.)  
478 Wiley, 71-99 (2010).
- 479 50. Mayer, L. Quinn, T. Wadsley, J. & Stadel, J. The Evolution of Gravitationally Unstable  
480 Protoplanetary Disks: Fragmentation and Possible Planet Formation. *Astrophys. J.* **609**, 1045-1064  
481 (2004).
- 482 51. Wertz, O. *et al.* VLT/SPHERE robust astrometry of the HR8799 planets at milliarcsecond-level  
483 accuracy. Orbital architecture analysis with PyAstrOFit. *Astron. Astrophys.* **598**, A83 (2017).
- 484 52. Machida, M. N. Inutsuka, S. & Matsumoto, T. Formation process of the circumstellar disk: Long-  
485 term simulations in the main accretion phase of star formation. *Astrophys. J.* **724**, 1006-1020 (2010).
- 486 53. Schneider, M. D. Cole S. Frenk, C. S. & Szapudi, I. Defining and cataloging exoplanets: the  
487 exoplanet.eu database. *Astron. Astrophys.* **523**, A79 (2011).
- 488 54. Mazeh, T. Latham, D. W. & Stefanik, R. P. Spectroscopic orbits for three binaries with low-mass  
489 companions and the distribution of secondary masses near the substellar limit. *Astrophys. J.* **466**, 415  
490 (1996).
- 491 55. Halbwachs, J. L. Arenou, F. Mayor, M. Udry, S. & Queloz, D. Exploring the brown dwarf desert  
492 with Hipparcos. *Astron. Astrophys.* **355**, 581-594 (2000).

- 493 56. Nidever, D. L. Marcy, G. W. & Butler, R. P. Radial velocities for 889 late-type stars. *Astrophys. J.*  
494 *Suppl.* **141**, 503-522 (2002).
- 495 57. Moutou, C. *et al.* The HARPS search for southern extra-solar planets. XV. Six long-period giant  
496 planets around BD -17 0063, HD 20868, HD 73267, HD 131664, HD 145377, and HD 153950.  
497 *Astron. Astrophys.* **496**, 513-519 (2009).
- 498 58. Bouchy, F. *et al.* The SOPHIE search for northern extrasolar planets. I. A companion around HD  
499 16760 with mass close to the planet/brown-dwarf transition. *Astron. Astrophys.* **505**, 853-858 (2009a).
- 500 59. Sahlmann, J. *et al.* Search for brown-dwarf companions of stars. *Astron. Astrophys.* **525**, A95 (2011).
- 501 60. Díaz, R. F. *et al.* The SOPHIE search for northern extrasolar planets. IV. Massive companions in the  
502 planet-brown dwarf boundary. *Astron. Astrophys.* **538**, A113 (2012).
- 503 61. Bouchy, F. *et al.* The SOPHIE search for northern extrasolar planets. VIII. Follow-up of ELODIE  
504 candidates: long-period brown-dwarf companions. *Astron. Astrophys.* **585**, A46 (2016).
- 505 62. Wilson, P. A. *et al.* The SOPHIE search for northern extrasolar planets. IX. Populating the brown  
506 dwarf desert. *Astron. Astrophys.* **588**, A144 (2016).
- 507 63. Santos, N. C. *et al.* SWEET-Cat: A catalogue of parameters for stars with exoplanets. I. New  
508 atmospheric parameters and masses for 48 stars with planets. *Astron. Astrophys.* **556**, A150 (2013).
- 509 64. Santos, N. C. Israelian, G. & Mayor, M. Spectroscopic [Fe/H] for 98 extra-solar planet-host stars.  
510 Exploring the probability of planet formation. *Astron. Astrophys.* **415**, 1153-1166 (2004).
- 511 65. Sousa, S. G. *et al.* Spectroscopic parameters for 451 stars in the HARPS GTO Planet Search Program.  
512 Stellar [Fe/H] and the frequency of exo-Neptunes. *Astron. Astrophys.* **487**, 373-381 (2008).
- 513 66. Brewer, J. M. Fischer, D. A. Valenti, J. A. & Piskunov, N. Spectral Properties of cool stars: extended

- 514 abundance analysis of 1,617 planet search stars. *Astrophys. J. Suppl.* **225**, 32 (2016).
- 515 67. Casagrande, L. *et al.* New constraints on the chemical evolution of the solar neighbourhood and  
516 Galactic disc(s). Improved astrophysical parameters for the Geneva-Copenhagen Survey. *Astron.  
517 Astrophys.* **530**, A138 (2011).
- 518 68. Torres, G. Winn, J. N. & Holman, M. J. Improved parameters for extrasolar transiting planets.  
519 *Astrophys. J.* **677**, 1324-1342 (2008).
- 520 69. Buchhave, L. A. *et al.* An abundance of small exoplanets around stars with a wide range of  
521 metallicities. *Nature* **486**, 375-377 (2012).
- 522 70. Weiss, L. M. *et al.* The mass of KOI-94d and a relation for planet radius, mass, and incident flux.  
523 *Astrophys. J.* **768**, 14 (2013).
- 524 71. Engmann, S. & Cousineau, D. Comparing distributions: the two-sample Anderson–Darling test as an  
525 alternative to the Kolmogorov-Smirnov test. *J. of Appl. Quant. Meth.* **6**, No.3 (2011).
- 526 72. Anderson, T. W. & Darling, D. A. Asymptotic theory of certain “Goodness of Fit” criteria based on  
527 stochastic processes. *Ann. Math. Statist.* **23**, 193-212 (1952).
- 528 73. Fraley, C. & Raftery, A. E. Model-based clustering, discriminant analysis, and density estimation. *J.  
529 Am. Stat. Assoc.* **97**, 611 (2012).
- 530 74. Fraley, C. Raftery, A. E. Murphy, T. B. & Scrucca, L. mclust Version 4 for R: Normal mixture  
531 modeling for model-based clustering, classification, and density estimation. Technical report No. 597,  
532 Department of Statistics, University of Washington (2012).
- 533 75. Schwarz, G. E. Estimating the dimension of a model. *Ann. Stat.*, 6 461-464 (1978).
- 534 76. Saar, S. H. Butler, R. P. Marcy, G. W. Magnetic Activity-Related Radial Velocity Variations in Cool

- 535 Stars: First Results from the Lick Extrasolar Planet Survey. *Astrophys. J.* **498**, 153-157 (1998).
- 536 77. Wright, J. T. Radial velocity jitters in stars from the California and Carnegie planet search at Keck
- 537 Observatory. *Pub. Astron. Soc. Pacific* **117**, 657-664 (2005).
- 538 78. Hekker, S. Reffert, S. Quirrenbach, A. et al. Precise radial velocities of giant stars. I. Stable stars.
- 539 *Astron. Astrophys.* **454**, 943-949 (2006).

540

541 **Acknowledgements**

542 First, the author is grateful for the continuous and extensive work conducted on radial velocity surveys  
543 and host-star characterization. In particular, of the various researchers involved with these projects, the  
544 author would like to thank the team members who constructed the SWEET-Cat and the Exoplanet.eu  
545 catalogues for the use of all exoplanet researchers. The author also acknowledges theoretical studies of  
546 the planetary formation processes that have been cited in this study. Especially, the author expresses  
547 deepest gratitude to Dr. Mordasini for releasing important results on planetary population synthesis,  
548 which were used for comparison with the observation result. The author would like to thank Dr.  
549 Schlaufman for developing crucial statistical analysis for this study. Finally, the author deeply  
550 appreciates anonymous referees for valuable comments, which lead to great improvement of this study.

551

552 **Author contributions statement**

553 The author constructed the samples, analysed the results, and wrote the manuscript.

554

555 **Competing financial interests**

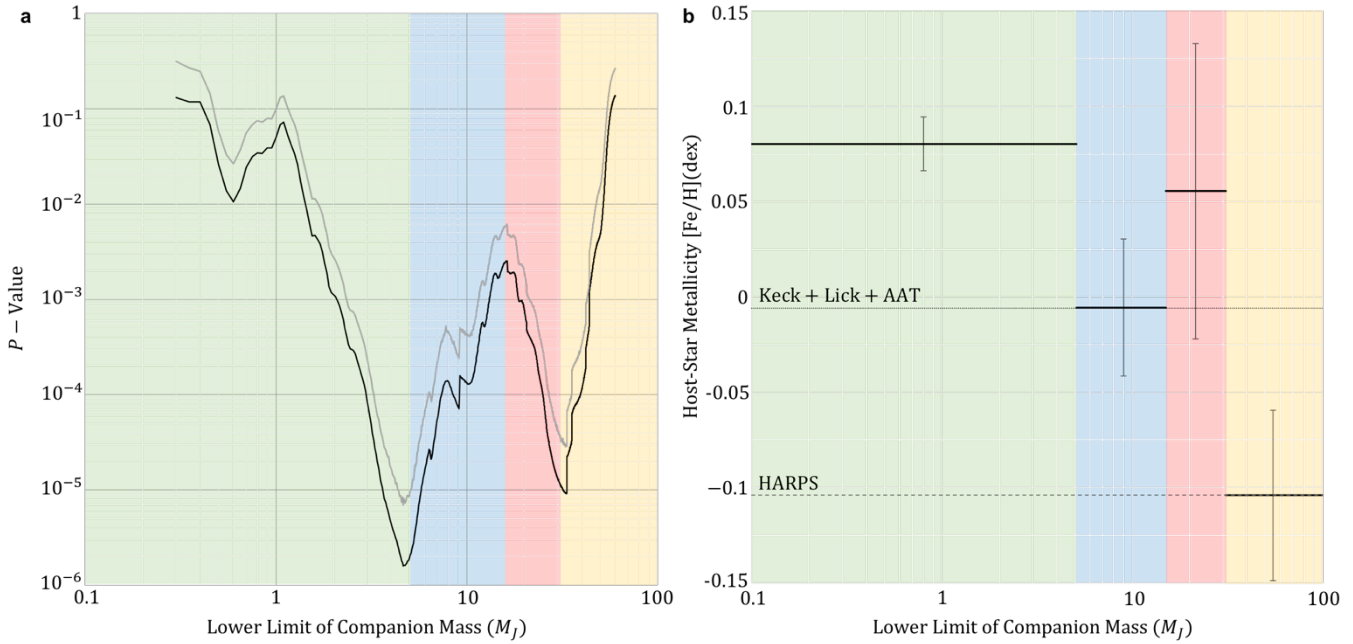
556 The author declares no competing financial interests.

557

558      **Correspondence** and request for material should be addressed to \*\*\*.

559

560



561

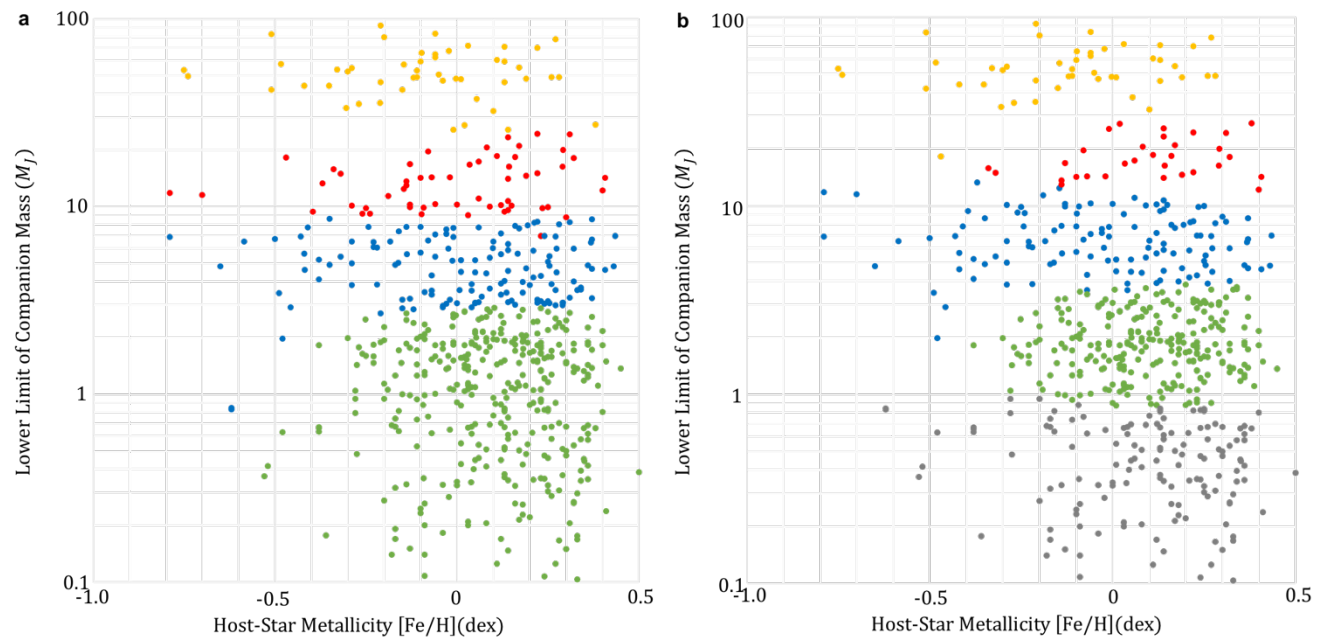
562 **Figure 1: Multiple populations of gaseous objects in terms of host-star metallicities.**

563 **a,** Result of two-sample Anderson–Darling test result for the 589 gaseous objects extracted from all the  
 564 722 samples. The lower boundary mass of the gaseous object is set to 0.1 Jupiter-mass. The  $P$ -values  
 565 changes from 0.3 to 60 Jupiter-mass in steps of 0.05 Jupiter-mass. The black line represents the mean  $P$ -  
 566 value averaged over 100000 calculations for each step. The grey line represents the 1-sigma upper limit  
 567 of the  $P$ -value and accounts for the measurement errors on the host-star metallicities and the companion  
 568 mass. The green, blue, red and yellow areas indicate the four-mass regimes, intermediate-mass planets,  
 569 massive planets, very massive planets and brown-dwarfs, respectively.

570 **b,** Model for the 589 gaseous objects and mean host-star metallicities. The lower boundary mass is set to  
 571 0.1 Jupiter-mass. The optimum model indicates that the 589 gaseous samples are divided into four bins:  
 572  $0.1 \leq M_p < 5M_J$ ,  $5 \leq M_p < 15M_J$ ,  $15 \leq M_p < 31M_J$  and  $31M_J \leq M_p$ , where  $M_J$  is the Jupiter-mass.  
 573 The mean metallicity and its standard deviation for each bin are shown. Dashed and dotted lines show the  
 574 average metallicities for volume-limited samples of HARPS<sup>31</sup> and Keck, Lick and AAT<sup>32</sup> radial velocity  
 575 surveys, respectively.

576

577



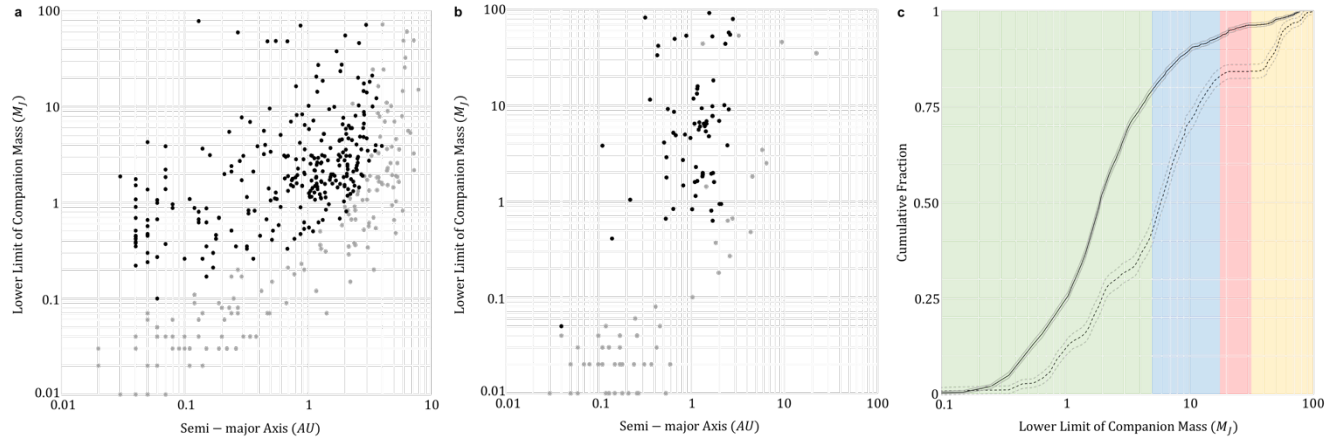
578

579 **Figure 2: Two appropriate models for the 589 gaseous objects.**

580 **a,** Four-component model for the 589 gaseous samples. The Gaussian mixture models with the number of  
581 components ranging from 1 to 8 are fit to the distribution of the host-star metallicities and the companion  
582 masses. The best model is selected based on the Bayesian Information Criterion (see Method section).  
583 The four-component model is selected from 40.1% of the 10,000 calculations.

584 **b,** Five-component model for the 589 gaseous samples. The five-component model is selected from 40.9%  
585 of the iterations.

586



587

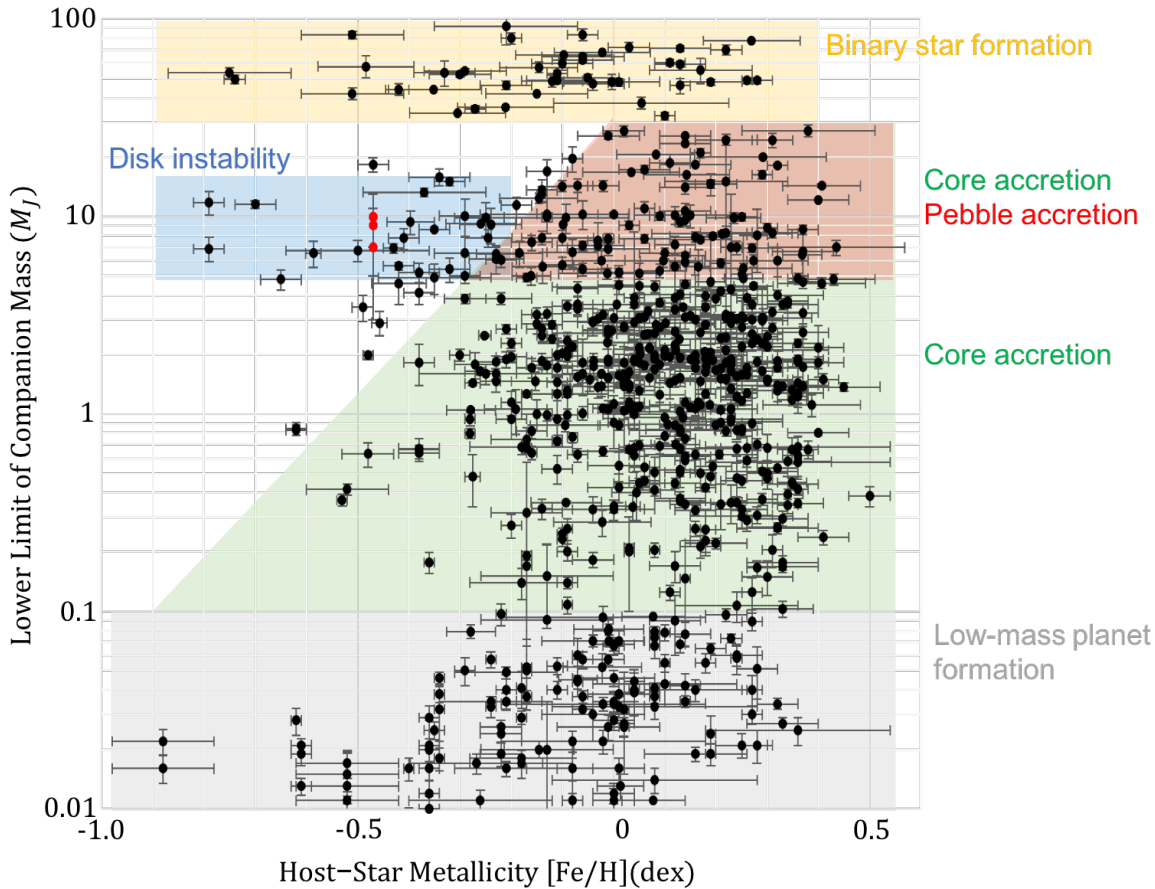
588 **Figure 3. Two planet deserts around metal-poor stars.**

589 **a**, Semi-major axis and companion mass distribution of the samples (black and grey dots) orbiting solar-  
590 metallicity and metal-rich stars ( $[Fe/H] \geq 0$ ). The black dots represent the samples, which can be detected  
591 by more than half of the radial velocity observations around the metal-poor stars (see Method section).

592 **b**, Semi-major axis and companion mass distribution of the samples (black and grey dots) orbiting metal-  
593 poor stars ( $[Fe/H] \leq -0.2$ ). The black dots are the same as those in panel (a).

594 **c**, Cumulative mass distributions for the two subsamples shown as the black dots in panels (a) and (b).  
595 The black solid and dashed lines are the cumulative mass functions of the subsamples orbiting non-metal-  
596 poor stars ( $[Fe/H] \geq 0$ ) and metal-poor stars ( $[Fe/H] \leq -0.2$ ). The grey solid and dashed lines represent  
597 the uncertainties of the two cumulative mass distributions around the non-metal-poor stars and metal-poor  
598 stars, respectively. The green, blue, red and yellow areas indicate the four-mass regimes, intermediate-  
599 mass planets, massive planets and brown-dwarfs, respectively.

600



601

602 **Figure 4. Distribution of host-star metallicities and companion masses for all 722 samples.**

603 Comparison of all samples with expectations from core accretion, pebble accretion and disk instability  
 604 theories in terms of host-star metallicity and planetary mass distributions. The blue and red dots indicate  
 605 the samples listed in Extended Data Table 2 and the four planets orbiting HR 8799, respectively. The green,  
 606 red and blue regions indicate the objects formed by core accretion, pebble accretion and disk instability,  
 607 respectively, given that the pebble accretion contributes to the formation of massive planets and very  
 608 massive planets orbiting metal-rich stars and the metallicity dependency of pebble accretion is the same  
 609 as that of core accretion. The two critical metallicities for the core accretion model are set to  $-0.9$  and  $0.0$   
 610 dex<sup>9</sup> (see Supplementary Information). The error bars indicate the 1-sigma measurement errors listed in  
 611 Extended Data Tables 1 and 2.  
 612

613    **Nature Behind Multiple Populations of Extrasolar Gaseous**

614    **Objects**

615    ***Supplementary Information***

616

617    **Planetary formation scenarios**

618    Here I briefly describe the planetary formation scenarios of core accretion<sup>2,3,4,79</sup>, pebble accretion<sup>27,28</sup> and  
619    gravitational disk instability<sup>5,6,7</sup> to discuss the final masses of planets and the two critical disk metallicities  
620    of core-accreted planets. The core accretion scenario is primarily divided into three phases: first, a core  
621    composed of heavy elements is built via the accumulation of planetesimals in its feeding zone<sup>80</sup>. Second,  
622    a gaseous envelope surrounding the core begins to develop during the accumulation of planetesimals,  
623    maintaining a balance between pressure gradient force and gravity of the core; therefore, the gas accretion  
624    rate is controlled by the accretion energy of the planetesimals. Finally, once the total mass of the core and  
625    envelope reaches to the critical core mass of ~10 times the Earth's mass<sup>3,81</sup>, the gas in the protoplanetary  
626    disk rapidly accretes onto the massive core. Therefore, the gaseous proto-planet can grow to the mass of  
627    Jupiter, except when the timescale for the core growth to the critical core mass is longer than the disk  
628    lifetime and the core isolation mass is less than the critical core mass. These two conditions for the  
629    formation of gas giants lead to one of the two critical metallicities, as will be discussed later. In addition  
630    to the original core-accretion model, the gas accretion rate of the proto-planet is limited by its gravitational  
631    scattering<sup>82,83</sup> and/or the accretion rate of the disk<sup>84,34,46</sup> in the final state. As will be introduced in the next  
632    section, the final masses of the core-accreted planets depend on the accretion rate of the gaseous proto-  
633    planet in the final state.

634 However, two critical issues still remain with core formation via the standard core accretion process. First,  
635 particles and pebbles with sizes ranging from *mm* to *cm* experience rapid radial migration due to gas drag.  
636 Because the migration timescales for *m*-sized particles are much shorter than those of planetesimal  
637 formation<sup>85,86</sup>, the rapid radial drifts of the *m*-sized particles prevent planetesimals with *km* sizes from  
638 forming at the onset of the standard core accretion scenario. Second, even if the *m*-sized barrier is  
639 overcome and the *km*-sized planetesimals form, it remains unclear whether the cores reach to the critical  
640 core mass before the gas disk dissipates. This is because planetesimals near an embryo are cleared through  
641 gravitational interaction between the embryo and the planetesimals, and the core growth rate decreases<sup>87</sup>.  
642 The pebble accretion scenario has recently been proposed to provide a solution for the two critical issues  
643 mentioned above. The pebble accretion model occurs mainly in two phases: in the first phase,  
644 planetesimals directly form from 10-*cm*-size particles through the streaming instability<sup>88</sup>. After the  
645 formation of large planetesimals, the remaining pebbles accrete onto the largest planetesimal very rapidly  
646 due to its impact parameter, which is as large as the radius of the entire Hill sphere<sup>27,28</sup>. The core reaches  
647 the critical core mass within the disk lifetime. Thus, pebble accretion helps to form the cores, especially  
648 in the outer region beyond a few AU, where the timescale for core growth via the standard core accretion  
649 is much longer and potentially contributes to the formation of planets more massive than a few Jupiter-  
650 mass.  
651 In the disk instability scenario, the disk is gravitationally unstable and fragments into several dense cores,  
652 provided the self-gravity of the disk prevails over the stabilization due to its pressure gradient (i.e.,  
653 Toomre-Q value<sup>89</sup> < 1) and the cooling timescale is comparable to the dynamical timescale<sup>90,91</sup>. Gaseous  
654 proto-planets are formed via contraction of the dense cores over a short timescale.  
655  
656

657    **Final masses of planets formed via core accretion and disk instability**

658    The planetary mass function is thought to be an important tracer of the planet formation history<sup>39,92</sup>. That  
659    is, although the number distribution of planets formed via the core accretion process gradually decreases  
660    with increasing planetary mass, disk instability leads to the formation of objects more massive than the  
661    Jeans mass or the opacity-limited mass<sup>93</sup>. In other words, planets formed as a result of core accretion and  
662    disk instability have upper and lower limits, respectively, in terms of the object mass<sup>39</sup>. Note that the  
663    opacity-limited mass is lighter than the Jeans mass because longer cooling times due to the high opacity  
664    of the gas prevent gas accretion onto proto-gaseous objects.

665    First, I discuss the final masses of the core-accretion-formed planets. In the final phase of the core  
666    accretion scenario, the accretion rate onto a gaseous proto-planet gradually decreases<sup>82,83</sup>, because of the  
667    larger gravitational scattering of the gaseous proto-planet against the pressure gradient and the viscous  
668    diffusion of the disk gas. When the gravitational scattering is balanced by the pressure gradient or viscous  
669    diffusion, the proto-planet opens a gap in the disk and gas accretion onto the proto-planet is significantly  
670    reduced. In this case, the final masses of the planets are not larger than  $10 M_J$ <sup>39</sup>. Conversely, the final mass  
671    of an object formed via core accretion is potentially up to  $30 M_J$ <sup>33,34</sup>, provided that the planet growth rate  
672    is limited by the mass flux of the accretion disk<sup>84,46</sup>. In fact, a previous population synthesis<sup>33</sup> predicted a  
673    continuous decrease in the planetary mass and is in good agreement with the results of radial velocity  
674    observations<sup>94</sup>. Finally, I remark on two points of the planetary mass function. The first is that the timescale  
675    of the planet growth is thought to be longer for larger planetary masses. The second is that, as discussed  
676    in a later section, the final masses of the planets formed by the core accretion process depend on disk  
677    metallicity.

678    Next, I describe the final mass of disk-instability-formed planets. According to a local perturbative  
679    stability analysis for an arbitrarily thin disk<sup>89</sup>, because the scale of the perturbation is shorter than the

680 Toomre critical wavelength  $\lambda_{crit}$  and longer than the Jeans scale  $\lambda_{Jeans}$ , the masses of the planets formed  
681 via disk instability may be roughly estimated as<sup>49</sup>

682 
$$\frac{2}{3}\pi\Sigma\left(\frac{\lambda_{Jeans}}{2}\right)^2 \leq M_p \leq \frac{2}{3}\pi\Sigma\left(\frac{\lambda_{crit}}{2}\right)^2, \quad (s1)$$

683 where  $\Sigma$  is the surface mass density of the disk. The lower and upper limits of the planets formed via disk  
684 instability are a few Jupiter-mass<sup>39</sup> and 10 Jupiter-mass, respectively, given that the Kusaka model<sup>95</sup> and  
685 more than ten times the MMSN model are applied as distributions of disk temperature and gas density,  
686 respectively. However, the above considerations are validated in the linear regime, and the analytic  
687 perturbations are confined to the symmetric perturbations. The stability analysis for a disk with a finite  
688 thickness can be revealed via numerical simulations. According to some numerical simulations of disk  
689 instability<sup>6,7,49,50</sup>, the disk fragments into several clumps with masses ranging from a few to ten Jupiter-  
690 mass, corresponding to the order of the Jeans and critical masses roughly estimated above. Note that there  
691 is some uncertainty regarding the final masses of the disk-instability-formed planets because these masses  
692 depend on the semi-major axes<sup>96</sup> at which the gas giants are formed, disk evolution<sup>52</sup>, and certain disk  
693 properties, such as disk mass, disk temperature, and opacity<sup>10,11</sup>.

694

## 695 Two critical metallicities for core-accretion-formed planets

696 There are most likely two critical metallicities related to the core accretion scenario: metallicity for the  
697 formation of a gas giant and that for the growth of the gas giant to the disk mass corresponding to a brown-  
698 dwarf mass. The first critical metallicity can be estimated from the two requirements for gas giant  
699 formation via the core accretion process. When the following two requirements are simultaneously  
700 satisfied, runaway gas accretion onto the core occurs. The first requirement is that the isolation mass<sup>80</sup>,  
701 which is almost equal to the amount of planetesimals in the core feeding zone, is larger than the critical

702 core mass<sup>3,81</sup>. The second requirement is that the core grows to the critical core mass before the gas is  
703 depleted. Because the isolation mass is more massive at greater distances from the central star, the former  
704 criterion yields the inner boundary of the region in which gas giants can be formed. By contrast, the latter  
705 constrains the outer boundary because the core growth timescale is proportional to the Kepler orbital  
706 period. Therefore, gas giant formation does not occur in a planetary system if the gas giant formation  
707 region is not produced. By requiring that the inner boundary coincide with the outer boundary, the critical  
708 metallicity around a  $1 M_{\odot}$  star can be written as follows<sup>35</sup>:

$$709 \quad [\text{Fe/H}]_{crit} \sim -0.92 + \log \left[ \left( \frac{f_g}{10} \right)^{\frac{17}{16}} \left( \frac{\tau_{disk}}{10^7 \text{year}} \right)^{-\frac{5}{32}} \left( \frac{M_{c,crit}}{10 M_{\oplus}} \right)^{\frac{59}{96}} \right], \quad (\text{s2})$$

710 where  $f_g$  is the scaling factor for the gas surface density of the MMSN model,  $\tau_{disk}$  is the gas depletion  
711 timescale,  $M_{c,crit}$  is the critical core mass, and  $M_{\oplus}$  is the mass of the Earth mass.

712 The second critical metallicity relates to the final masses of the planets formed via core accretion process.  
713 Several numerical simulations<sup>29,30</sup> show that proto-gaseous planets can acquire disk mass when the growth  
714 rate of these planets is limited by the accretion rate in the disk. Because the disk accretion rate continuously  
715 decreases via disk depletion, the planets are thought to have a wide range of masses from Saturn mass to  
716 the disk mass. The final mass of the planet is thought to be characterized by the starting time of rapid gas  
717 accretion onto the core. It is likely that one of the determining factors of the final mass is disk metallicity.  
718 Because the growth timescale of the core to the critical core mass depends on disk metallicity, gas  
719 accretion onto the core begins at an earlier stage of disk evolution if the disk metallicity is higher.  
720 Therefore, the planetary mass more easily reaches a brown-dwarf value in a disk with higher metallicity.

721 A previous population synthesis<sup>9</sup> also demonstrated that the upper limit of the planetary mass increases  
722 continuously with increasing disk metallicity. For example, the critical metallicity for the growth of a  
723 planet to 31 Jupiter-mass, corresponding to the boundary shown in Figure 1a, is approximately 0.0 dex.

724 Therefore, this expectation regarding the relationship between the final mass and the disk metallicity is  
725 nearly consistent with that of the above-mentioned previous study<sup>9</sup>. It is difficult to quantitatively estimate  
726 the second critical metallicity in the same manner as the first, because gas accretion onto the proto-planet  
727 depends on both global disk evolution and planet-disk interaction. In addition, there are no negligible  
728 discrepancies among the several numerical simulations<sup>34,48</sup> in terms of the planetary gas accretion rate.

729

## 730 References

- 731 79. Bodenheimer, P. & Pollack, J. B. Calculations of the accretion and evolution of giant planets The  
732 effects of solid cores. *Icarus* **67**, 391-408 (1986).
- 733 80. Kokubo, E. & Ida, S. Formation of protoplanet systems and diversity of planetary systems. *Astrophys.*  
734 *J.* **581**, 660-680 (2002).
- 735 81. Ikoma, M. Nakazawa, K. & Emori, H. Formation of giant planets: Dependences on core accretion  
736 rate and grain opacity. *Astrophys. J.* **537**, 1013-1025 (2000).
- 737 82. Lubow, S. H. Seibert, M. & Artymowicz, P. Disk Accretion onto High-Mass Planets. *Astrophys. J.*  
738 **526**, 1101-1012 (1999).
- 739 83. D'Angelo, G. Henning, T. Kley, W. Nested-grid calculations of disk-planet interaction. *Astron.*  
740 *Astrophys.* **385**, 647-670 (2002).
- 741 84. Tanigawa, T. & Ikoma, M. A Systematic Study of the Final Masses of Gas Giant Planets. *Astrophys.*  
742 *J.* **667**, 557-570 (2007).
- 743 85. Adachi, I. Hayashi, C. & Nakazawa, K. The gas drag effect on the elliptical motion of a solid body  
744 in the primordial solar nebula. *Prog. Theor. Phys.* **56**, 1756-1771 (1976).

- 745 86. Weidenschilling, S. J. Aerodynamics of solid bodies in the solar nebula. *Mon. Not. Roy. Astron. Soc.*
- 746 **180**, 57-70 (1977).
- 747 87. Levison, H. F. Thommes, E. & Duncan, M. J. Modeling the formation of giant planet cores. I.
- 748 evaluating key processes. *Astron. J.* **139**, 1297-1314 (2010).
- 749 88. Johansen, A. & Youdin, A. Protoplanetary disk turbulence driven by the streaming instability:
- 750 nonlinear saturation and particle concentration. *Astrophys. J.* **662**, 627-641 (2007).
- 751 89. Toomre, A. On the Gravitational Stability of a Disk of Stars. *Astrophys. J.* **139**, 1217-1238 (1964).
- 752 90. Gammie, C. F. Nonlinear Outcome of Gravitational Instability in Cooling, Gaseous Disks. *Astrophys.*
- 753 *J.* **553**, 174-183 (2001).
- 754 91. Rice, W. K. M. Lodato, G. & Armitage, P. J. Investigating fragmentation conditions in self-
- 755 gravitating accretion discs. *Mon. Not. Roy. Astron. Soc.* **364**, 56-60 (2005).
- 756 92. Ribas, I. & Miralda-Escudé, J. The eccentricity-mass distribution of exoplanets: signatures of
- 757 different formation mechanisms? *Astron. Astrophys.* **464**, 779-785 (2007).
- 758 93. Rees, M. J. Opacity-limited hierarchical fragmentation and the masses of protostars. *Mon. Not. Roy.*
- 759 *Astron. Soc.* **176**, 483-486 (1976).
- 760 94. Marcy, G. *et al.* Observed Properties of Exoplanets: Masses, Orbits, and Metallicities. *Prog. Thoer.*
- 761 *Phys. Suppl.* **158**, 24-42 (2005b).
- 762 95. Kusaka, T. Nakano, T. & Hayashi, C. Growth of solid particles in the primordial solar nebula. *Prog.*
- 763 *Theor. Phys.* **44**, 1580-1595 (1970).
- 764 96. Stamatellos, D. & Whitworth, A. P. The properties of brown dwarfs and low-mass hydrogen-burning
- 765 stars formed by disk fragmentation. *Mon. Not. Roy. Astron. Soc.* **392**, 413-427 (2009).

- 766 97. Affer, L. *et al.* The HADES RV programme with HARPS-N@TNG GJ 3998: An early M-dwarf  
767 hosting a system of super-Earths. *Astron. Astrophys.* **593**, A117 (2016).
- 768 98. Ammler-von Eiff, M. *et al.* A homogeneous spectroscopic analysis of host stars of transiting planets.  
769 *Astron. Astrophys.* **507**, 523-530 (2009).
- 770 99. Andreassen, D. T. *et al.* Accepted for publication in *Astron. Astrophys.* (private communication with  
771 Dr. Santos).
- 772 100. Anglada-Escudé, G. *et al.* Astrometry and radial velocities of the planet host M Dwarf GJ 317: New  
773 trigonometric distance, metallicity, and upper limit to the mass of GJ 317b. *Astrophys. J.* **746**, 37  
774 (2012a).
- 775 101. Anglada-Escudé, G. & Tuomi, M. A planetary system with gas giants and super-Earths around the  
776 nearby M dwarf GJ 676A. Optimizing data analysis techniques for the detection of multi-planetary  
777 systems. *Astron. Astrophys.* **548**, A58 (2012b).
- 778 102. Anglada-Escudé, G. *et al.* A dynamically-packed planetary system around GJ 667C with three super-  
779 Earths in its habitable zone. *Astron. Astrophys.* **556**, A126 (2013).
- 780 103. Anglada-Escudé, G. *et al.* Two planets around Kapteyn's star: a cold and a temperate super-Earth  
781 orbiting the nearest halo red dwarf. *Mon. Not. Roy. Astron. Soc.* **443**, 89-93 (2014).
- 782 104. Apps, K. *et al.* Two planets around Kapteyn's star: M2K: I. A Jupiter-Mass Planet Orbiting the M3V  
783 Star HIP 79431. *Pub. Astron. Soc. Pacific* **122**, 156-161 (2010).
- 784 105. Arriagada, P. *et al.* Five long-period extrasolar planets in eccentric orbits from the Magellan Planet  
785 Search Program. *Astrophys. J.* **711**, 1229-1235 (2010).

- 786 106. Astudillo-Defru, N. *et al.* The HARPS search for southern extra-solar planets. XXXVI. Planetary  
787 systems and stellar activity of the M dwarfs GJ 3293, GJ 3341, and GJ 3543. *Astron. Astrophys.* **575**,  
788 A119 (2015).
- 789 107. Baluev, R. & Beaugé, C. Possible solution to the riddle of HD 82943 multiplanet system: the three-  
790 planet resonance 1:2:5? *Mon. Not. Roy. Astron. Soc.* **439**, 673 (2014).
- 791 108. Barbieri, C. *et al.* Characterization of the HD 17156 planetary system. *Astron. Astrophys.* **503**, 601-  
792 612 (2009).
- 793 109. Bedell, M. *et al.* The Solar Twin Planet Search. II. A Jupiter twin around a solar twin. *Astron.*  
794 *Astrophys.* **581**, A34 (2015).
- 795 110. Boisse, I. *et al.* The SOPHIE search for northern extrasolar planets. III. A Jupiter-mass companion  
796 around HD 109246. *Astron. Astrophys.* **523**, A88 (2010).
- 797 111. Boisse, I. *et al.* The SOPHIE search for northern extrasolar planets. V. Follow-up of ELODIE  
798 candidates: Jupiter-analogs around Sun-like stars. *Astron. Astrophys.* **545**, A55 (2012).
- 799 112. Bonfils, X. *et al.* The HARPS search for southern extra-solar planets. X. A  $m \sin i = 11 M_{\oplus}$  planet  
800 around the nearby spotted M dwarf GJ 674. *Astron. Astrophys.* **474**, 293-299 (2007).
- 801 113. Bonfils, X. *et al.* A short-period super-Earth orbiting the M2.5 dwarf GJ 3634. Detection with  
802 HARPS velocimetry and transit search with Spitzer photometry. *Astron. Astrophys.* **528**, A111 (2011).
- 803 114. Bonfils, X. *et al.* The HARPS search for southern extra-solar planets. XXXIV. A planetary system  
804 around the nearby M dwarf GJ 163, with a super-Earth possibly in the habitable zone. *Astron.*  
805 *Astrophys.* **556**, A110 (2013).

- 806 115. Bonsor, A. *et al.* Spatially resolved images of dust belt(s) around the planet-hosting subgiant  $\kappa$  CrB.  
807 *Mon. Not. Roy. Astron. Soc.* **431**, 3025-3035 (2013).
- 808 116. Borgniet, S. *et al.* Extrasolar planets and brown dwarfs around A-F type stars. VIII. A giant planet  
809 orbiting the young star HD 113337. *Astron. Astrophys.* **561**, A65 (2014).
- 810 117. Bouchy, F. *et al.* ELODIE metallicity-biased search for transiting Hot Jupiters. II. A very hot Jupiter  
811 transiting the bright K star HD 189733. *Astron. Astrophys.* **444**, 15-19 (2005).
- 812 118. Bouchy, F. *et al.* The HARPS search for southern extra-solar planets XVII. Super-Earth and Neptune-  
813 mass planets in multiple planet systems HD 47186 and HD 181433. *Astron. Astrophys.* **496**, 527-531  
814 (2009).
- 815 119. Bowler, B. *et al.* Retired A Stars and Their Companions. III. Comparing the Mass-Period  
816 Distributions of Planets Around A-Type Stars and Sun-Like Stars. *Astrophys. J.* **709**, 396-410 (2010).
- 817 120. Brogi, M. *et al.* The signature of orbital motion from the dayside of the planet  $\tau$  Boötis b. *Nature* **486**,  
818 502-504 (2012).
- 819 121. Brucalassi, A. *et al.* Three planetary companions around M 67 stars. *Astron. Astrophys.* **561**, L9  
820 (2014).
- 821 122. Butler, R. P. *et al.* Catalog of nearby exoplanets. *Astrophys. J.* **646**, 505-522 (2006).
- 822 123. Carter, J. A. Winn, J. N. Gilliland, R. & Holman, M. J. Near-Infrared Transit Photometry of the  
823 Exoplanet HD 149026b. *Astrophys. J.* **696**, 241-253 (2009).
- 824 124. Correia, A. C. M. *et al.* The CORALIE survey for southern extra-solar planets. XIII. A pair of planets  
825 around HD 202206 or a circumbinary planet? *Astron. Astrophys.* **440**, 751-758 (2005).

- 826 125. Correia, A. C. M. *et al.* The HARPS search for southern extra-solar planets. XVI. HD 45364, a pair  
827 of planets in a 3:2 mean motion resonance. *Astron. Astrophys.* **440**, 521-526 (2009).
- 828 126. Courcol, B. *et al.* The SOPHIE search for northern extrasolar planets. VII. A warm Neptune orbiting  
829 HD 164595. *Astron. Astrophys.* **581**, A38 (2015).
- 830 127. Curiel, S. *et al.* A fourth planet orbiting v Andromedae. *Astron. Astrophys.* **525**, A78 (2011).
- 831 128. Da Silva, R. *et al.* ELODIE metallicity-biased search for transiting hot Jupiters I. Two hot Jupiters  
832 orbiting the slightly evolved stars HD 118203 and HD 149143. *Astron. Astrophys.* **446**, 717-722  
833 (2006).
- 834 129. Da Silva, R. *et al.* ELODIE metallicity-biased search for transiting hot Jupiters. IV. Intermediate  
835 period planets orbiting the stars HD 43691 and HD 132406. *Astron. Astrophys.* **473**, 323-328 (2007).
- 836 130. Damasso, M. *et al.* The GAPS programme with HARPS-N at TNG. IX. The multi-planet system  
837 KELT-6: Detection of the planet KELT-6 c and measurement of the Rossiter-McLaughlin effect for  
838 KELT-6 b. *Astron. Astrophys.* **581**, L6 (2015).
- 839 131. Delfosse, X. *et al.* The HARPS search for southern extra-solar planets. XXXV. Super-Earths around  
840 the M-dwarf neighbors Gl 433 and Gl 667C. *Astron. Astrophys.* **553**, A8 (2013).
- 841 132. Delgado-Mena, E. Li depletion in solar analogues with exoplanets. Extending the sample. *Astron.*  
842 *Astrophys.* **562**, A92 (2014).
- 843 133. Desidera, S. *et al.* A giant planet in the triple system HD 132563. *Astron. Astrophys.* **533**, A90 (2011).
- 844 134. Desidera, S. *et al.* The GAPS programme with HARPS-N at TNG IV. A planetary system around  
845 XO-2S. *Astron. Astrophys.* **567**, L6 (2014).

- 846 135. Desort, M. *et al.* Extrasolar planets and brown dwarfs around A-F type stars. V. A planetary system  
847 found with HARPS around the F6IV-V star HD 60532. *Astron. Astrophys.* **491**, 883-888 (2008).
- 848 136. Díaz, R. F. *et al.* The SOPHIE search for northern extrasolar planets. IV. Massive companions in the  
849 planet-brown dwarf boundary. *Astron. Astrophys.* **538**, A113 (2012).
- 850 137. Díaz, R. F. *et al.* The SOPHIE search for northern extrasolar planets. XI. Three new companions and  
851 an orbit update: Giant planets in the habitable zone. *Astron. Astrophys.* **591**, A146 (2016).
- 852 138. Döllinger, M. P. *et al.* Discovery of a planet around the K giant star 4 Ursae Majoris. *Astron.*  
853 *Astrophys.* **472**, 649-652 (2007).
- 854 139. Döllinger, M. P. *et al.* Planetary companion candidates around the K giant stars 42 Draconis and HD  
855 139357. *Astron. Astrophys.* **499**, 935-942 (2009).
- 856 140. Dumusque, X. *et al.* The HARPS search for southern extra-solar planets. XXX. Planetary systems  
857 around stars with solar-like magnetic cycles and short-term activity variation. *Astron. Astrophys.* **535**,  
858 A55 (2011).
- 859 141. Dumusque, X. *et al.* An Earth-mass planet orbiting α Centauri B. *Nature* **491**, 207-211 (2012).
- 860 142. Eastman, J. D. *et al.* KELT-4Ab: An inflated hot Jupiter transiting the bright ( $V \sim 10$ ) component of  
861 a hierarchical triple. *Astron. J.* **151**, 45 (2016).
- 862 143. Eggenberger, A. *et al.* The CORALIE survey for southern extrasolar planets. XIV. HD 142022 b: a  
863 long-period planetary companion in a wide binary. *Astron. Astrophys.* **447**, 1159-1163 (2006).
- 864 144. Endl, M. Cochran, W. D. Wittenmyer, R. A. & Hatzes, A. P. Determination of the Orbit of the  
865 Planetary Companion to the Metal-Rich Star HD 45350. *Astrophys. J.* **131**, 3131-3134 (2006).

- 866 145. Endl, M. *et al.* Revisiting  $\rho^1$  Cancri e: A New Mass Determination of the Transiting Super-Earth.  
867 *Astrophys. J.* **759**, 19 (2012).
- 868 146. Endl, M. *et al.* Kepler-424 b: A "lonely" hot Jupiter that found a companion. *Astrophys. J.* **795**, 151  
869 (2014).
- 870 147. Endl, M. *et al.* Two new long-period giant planets from the McDonald Observatory Planet Search  
871 and two stars with long-period radial velocity signals related to stellar activity cycles. *Astrophys. J.*  
872 **818**, 34 (2016).
- 873 148. Feng, Y. K. *et al.* The California Planet Survey IV: A Planet Orbiting the Giant Star HD 145934 and  
874 Updates to Seven Systems with Long-period Planets. *Astrophys. J.* **800**, 22 (2015).
- 875 149. Feroz, F. Balan, S. T. & Hobson, M. P. Bayesian evidence for two companions orbiting HIP 5158.  
876 *Mon. Not. Roy. Astron. Soc.* **416**, 104-108 (2011).
- 877 150. Fischer, D. A. *et al.* The N2K Consortium. III. Short-period planets orbiting HD 149143 and HD  
878 109749. *Astrophys. J.* **637**, 1094-1101 (2006).
- 879 151. Fischer, D. A. *et al.* Five intermediate-period planets from the N2K sample. *Astrophys. J.* **669**, 1336-  
880 1344 (2007).
- 881 152. Fischer, D. A. *et al.* Five planets and an independent confirmation of HD 196885Ab from Lick  
882 Observatory. *Astrophys. J.* **703**, 1545-1556 (2009).
- 883 153. Fischer, D. A. *et al.* M2K. II. A Triple-planet System Orbiting HIP 57274. *Astrophys. J.* **745**, 21  
884 (2012).
- 885 154. Forveille, T. *et al.* The HARPS search for southern extra-solar planets. XIV. Gl 176b, a super-Earth  
886 rather than a Neptune, and at a different period. *Astron. Astrophys.* **493**, 645-650 (2009).

- 887 155. Forveille, T. *et al.* The HARPS search for southern extra-solar planets XXXII. Only 4 planets in the  
888 Gl~581 system. Preprint at <https://arxiv.org/abs/1109.2505>.
- 889 156. Fulton, B. J. *et al.* Three Super-Earths Orbiting HD 7924. *Astrophys. J.* **805**, 175 (2015).
- 890 157. Fulton, B. J. *et al.* Three temperate Neptunes orbiting nearby stars. *Astrophys. J.* **830**, 46 (2016).
- 891 158. Galland, F. *et al.* Extrasolar planets and brown dwarfs around A-F type stars. II. A planet found with  
892 ELODIE around the F6V star HD 33564. *Astron. Astrophys.* **444**, 21-24 (2005).
- 893 159. Gettel, S. *et al.* Substellar-mass companions to the K-Giants HD 240237, BD+48 738, and HD 96127.  
894 *Astrophys. J.* **745**, 28 (2012a).
- 895 160. Gettel, S. *et al.* Planets around the K-Giants BD+20 274 and HD 219415. *Astrophys. J.* **756**, 53  
896 (2012b).
- 897 161. Gettel, S. *et al.* The Kepler-454 System: A small, not-rocky inner planet, a Jovian world, and a distant  
898 companion. *Astrophys. J.* **816**, 95 (2016).
- 899 162. Giguere, M. J. *et al.* A High-eccentricity Component in the Double-planet System around HD 163607  
900 and a Planet around HD 164509. *Astrophys. J.* **744**, 4 (2012).
- 901 163. Giguere, M. J. *et al.* Newly discovered planets orbiting HD 5319, HD 11506, HD 75784 and HD  
902 10442 from the N2K consortium. *Astrophys. J.* **779**, 89 (2015).
- 903 164. Gregory, F. C. & Fischer, D. A. A Bayesian periodogram finds evidence for three planets in  
904 47UrsaeMajoris. *Mon. Not. Roy. Astron. Soc.* **403**, 731-747 (2010).
- 905 165. Guenther, E. W. *et al.* A substellar component orbiting the F-star 30 Arietis B. *Astron. Astrophys.* **507**,  
906 1659-1665 (2009).

- 907 166. Haghighipour, N. *et al.* The Lick-Carnegie Exoplanet Survey: Saturn-mass planet in the habitable  
908 zone of the nearby M4V star HIP 57050. *Astrophys. J.* **715**, 271-276 (2010).
- 909 167. Haghighipour, N. *et al.* The Lick-Carnegie Survey: A New Two-planet System around the Star HD  
910 207832. *Astrophys. J.* **756**, 91 (2012).
- 911 168. Han, I. *et al.* Detection of a planetary companion around the giant star  $\gamma^1$  Leonis. *Astron. Astrophys.*  
912 **509**, A24 (2010).
- 913 169. Harakawa, H. *et al.* Detection of a low-eccentricity and super-massive planet to the subgiant HD  
914 38801. *Astrophys. J.* **715**, 550-553 (2010).
- 915 170. Harakawa, H. *et al.* Five new exoplanets orbiting three metal-rich, massive stars: Two-planet systems  
916 including long-period planets and an eccentric planet. *Astrophys. J.* **806**, 5 (2015).
- 917 171. Hartmann, M. *et al.* A Sub-stellar Companion around the F7 V Star HD 8673. *Astrophys. J.* **717**, 348-  
918 356 (2010).
- 919 172. Hatzes, A. P. *et al.* A Planetary Companion to  $\gamma$  Cephei A. *Astron. Astrophys.* **599**, 1383-1394 (2003).
- 920 173. Hatzes, A. P. *et al.* A giant planet around the massive giant star HD 13189. *Astron. Astrophys.* **437**,  
921 743-751 (2005).
- 922 174. Hatzes, A. P. *et al.* Confirmation of the planet hypothesis for the long-period radial velocity variations  
923 of  $\beta$  Geminorum. *Astron. Astrophys.* **457**, 335-341 (2006).
- 924 175. Hatzes, A. P. *et al.* Long-lived, long-period radial velocity variations in Aldebaran: A planetary  
925 companion and stellar activity. *Astron. Astrophys.* **580**, A31 (2015).
- 926 176. Hébrard, G. *et al.* The SOPHIE search for northern extrasolar planets. II. A multiple planet system  
927 around HD 9446. *Astron. Astrophys.* **513**, A69 (2010).

- 928 177. Hébrard, G. *et al.* The SOPHIE search for northern extrasolar planets. X. Detection and  
929 characterization of giant planets by the dozen. *Astron. Astrophys.* **588**, A145 (2016).
- 930 178. Hekker, S. & Meléndez, J. Precise radial velocities of giant stars. III. Spectroscopic stellar parameters.  
931 *Astron. Astrophys.* **475**, 1003-1009 (2007).
- 932 179. Hou, F. Goodman, J. & Hogg, D. W. The Probabilities of Orbital-Companion Models for Stellar  
933 Radial Velocity Data. Preprint at <https://arxiv.org/abs/1401.6128>.
- 934 180. Howard, A. W. *et al.* The California Planet Survey. I. Four new giant exoplanets. *Astrophys. J.* **721**,  
935 1467-1481 (2010).
- 936 181. Howard, A. W. *et al.* The NASA-UC Eta-Earth Program. II. A Planet Orbiting HD 156668 with a  
937 Minimum Mass of Four Earth Masses. *Astrophys. J.* **726**, 73 (2011a).
- 938 182. Howard, A. W. *et al.* The NASA-UC Eta-Earth Program. III. A Super-Earth Orbiting HD 97658 and  
939 a Neptune-mass Planet Orbiting Gl 785. *Astrophys. J.* **730**, 10 (2011b).
- 940 183. Howard, A. W. *et al.* HAT-P-17b,c: A Transiting, Eccentric, Hot Saturn and a Long-period, Cold  
941 Jupiter. *Astrophys. J.* **749**, 134 (2012).
- 942 184. Howard, A. W. *et al.* The NASA-UC-UH ETA-Earth Program. IV. A low-mass planet orbiting an M  
943 dwarf 3.6 PC from Earth. *Astrophys. J.* **794**, 51-59 (2014).
- 944 185. Hrudkova, M. *et al.* The discovery of a planetary candidate around the evolved low-mass Kepler  
945 giant star HD 175370. *Mon. Not. Roy. Astron. Soc.* **464**, 1018-1028 (2017).
- 946 186. Jenkins, J. S. *et al.* A hot Uranus orbiting the super metal-rich star HD 77338 and the metallicity-  
947 mass connection. *Astrophys. J.* **766**, 67 (2013).

- 948 187. Jenkins, J. S. *et al.* New planetary systems from the Calan-Hertfordshire Extrasolar Planet Search
- 949 and the core accretion mass limit. *Mon. Not. Roy. Astron. Soc.* **466**, 443-473 (2017).
- 950 188. Johnson, J. A. *et al.* The N2K Consortium. VI. Doppler shifts without templates and three new short-
- 951 period planets. *Astrophys. J.* **647**, 600-611 (2006).
- 952 189. Johnson J. A. *et al.* Retired A Stars and Their Companions: Exoplanets Orbiting Three Intermediate-
- 953 Mass Subgiants. *Astrophys. J.* **665**, 785-793 (2007).
- 954 190. Johnson J. A. *et al.* A Hot Jupiter Orbiting the  $1.7 M_{\text{sun}}$  Subgiant HD 102956. *Astrophys. J.* **721**,
- 955 153-157 (2010).
- 956 191. Johnson J. A. *et al.* Retired A Stars and their companions. VII. 18 new Jovian planets. *Astrophys. J.*
- 957 *Suppl.* **197**, 26 (2011).
- 958 192. Jones, H. R. A. *et al.* High-eccentricity planets from the Anglo-Australian Planet Search. *Mon. Not.*
- 959 *Roy. Astron. Soc.* **369**, 249-256 (2006).
- 960 193. Jones, H. R. A. *et al.* A long-period planet orbiting a nearby Sun-like star. *Mon. Not. Roy. Astron. Soc.*
- 961 **403**, 1703-1713 (2010).
- 962 194. Jones, M. I. *et al.* Study of the impact of the post-MS evolution of the host star on the orbits of close-
- 963 in planets. II. A giant planet in a close-in orbit around the RGB star HIP 63242. *Astron. Astrophys.*
- 964 **556**, A78 (2013).
- 965 195. Jones, M. I. *et al.* The properties of planets around giant stars. *Astron. Astrophys.* **566**, A113 (2014).
- 966 196. Jones, M. I. *et al.* A planetary system and a highly eccentric brown dwarf around the giant stars
- 967 HIP 67851 and HIP 97233. *Astron. Astrophys.* **573**, A3 (2015).

- 968 197. Jones, M. I. *et al.* Four new planets around giant stars and the mass-metallicity correlation of planet-  
969 hosting stars. *Astron. Astrophys.* **590**, A38 (2016).
- 970 198. Kane, S. R. *et al.* Revised Orbit and Transit Exclusion for HD 114762b. *Astrophys. J.* **735**, 41 (2011a).
- 971 199. Kane, S. R. *et al.* Stellar Variability of the Exoplanet Hosting Star HD 63454. *Astrophys. J.* **737**, 58  
972 (2011b).
- 973 200. Kane, S. R. *et al.* Limits on Stellar Companions to Exoplanet Host Stars with Eccentric Planets.  
974 *Astrophys. J.* **785**, 93 (2014).
- 975 201. Lee, B.-C. *et al.* A likely exoplanet orbiting the oscillating K-giant  $\alpha$  Arietis. *Astron. Astrophys.* **529**,  
976 A134 (2011).
- 977 202. Lee, B.-C. *et al.* Detection of an exoplanet around the evolved K giant HD 66141. *Astron. Astrophys.*  
978 **548**, A118 (2012).
- 979 203. Lee, B.-C., Han, I. & Park, M.-G. Planetary companions orbiting M giants HD 208527 and HD  
980 220074. *Astron. Astrophys.* **549**, A2 (2013).
- 981 204. Lee, B.-C. *et al.* Planetary companions in K giants  $\beta$  Cancri,  $\mu$  Leonis, and  $\beta$  Ursae Minoris. *Astron.*  
982 *Astrophys.* **566**, A67 (2014a).
- 983 205. Lee, B.-C. *et al.* Planetary companion in K Giant  $\sigma$  Persei. *Korean Astron. Soc.* **47**, 69-76 (2014b)
- 984 206. Lee, B.-C. *et al.* Search for exoplanet around northern circumpolar stars. Four planets around HD  
985 11755, HD 12648, HD 24064, and 8 Ursae Minoris. *Astron. Astrophys.* **584**, A79 (2015).
- 986 207. Liu, Y.-J. *et al.* A substellar companion to the intermediate-mass giant 11 Comae. *Astrophys. J.* **672**,  
987 553-557 (2008).

- 988 208. Liu, Y.-J. Sato, B. Zhao, G. Ando, H. A planetary companion orbiting the intermediate-mass G Giant
- 989 HD 173416. *Res. Astron. Astrophys.* **9**, 1-4 (2009).
- 990 209. Lo Curto, G. *et al.* The HARPS search for southern extra-solar planets. VII. A very hot Jupiter
- 991 orbiting HD 212301. *Astron. Astrophys.* **451**, 345-350 (2006).
- 992 210. Lo Curto, G. *et al.* The HARPS search for southern extra-solar planets XXII. Multiple planet systems
- 993 from the HARPS volume limited sample. *Astron. Astrophys.* **512**, A48 (2010).
- 994 211. Lo Curto, G. *et al.* The HARPS search for southern extra-solar planets . XXXII. New multi-planet
- 995 systems in the HARPS volume limited sample: a super-Earth and a Neptune in the habitable zone.
- 996 *Astron. Astrophys.* **551**, A59 (2013).
- 997 212. López-Morales, M. *et al.* Two Jupiter-mass planets orbiting HD 154672 and HD 205739. *Astrophys.*
- 998 *J.* **136**, 1901-1905 (2008).
- 999 213. Lovis, C. *et al.* The HARPS search for southern extra-solar planets. III. Three Saturn-mass planets
- 1000 around HD 93083, HD 101930 and HD 102117. *Astron. Astrophys.* **437**, 1121-1126 (2005).
- 1001 214. Lovis, C. *et al.* An extrasolar planetary system with three Neptune-mass planets. *Nature* **441**, 305-
- 1002 309 (2006).
- 1003 215. Lovis, C. & Mayor, M. Planets around evolved intermediate-mass stars I. Two substellar companions
- 1004 in the open clusters NGC 2423 and NGC 4349. *Astron. Astrophys.* **472**, 657-664 (2007).
- 1005 216. Lovis, C. *et al.* The HARPS search for southern extra-solar planets. XXVIII. Up to seven planets
- 1006 orbiting HD 10180: probing the architecture of low-mass planetary systems. *Astron. Astrophys.* **528**,
- 1007 A112 (2011).

- 1008 217. Ma, B. *et al.* Very low-mass stellar and substellar companions to solar-like stars from MARVELS  
1009 VI: a giant planet and a brown dwarf candidate in a close binary system HD 87646. *Astron. J.* **152**,  
1010 112 (2016).
- 1011 218. Malavolta, L. *et al.* The GAPS programme with HARPS-N at TNG. XI. Pr 0211 in M 44: the first  
1012 multi-planet system in an open cluster. *Astron. Astrophys.* **588**, A118 (2016).
- 1013 219. Maness, H. L. *et al.* The M Dwarf GJ 436 and its Neptune-Mass Planet. *Pub. Astron. Soc. Pacific*  
1014 **119**, 90-101 (2007).
- 1015 220. Marcy, G. W. *et al.* Masses, radii, and orbits of small kepler planets: The transition from gaseous to  
1016 rocky planets. *Astrophys. J. Suppl.* **210**, 20 (2014).
- 1017 221. Marmier, M. *et al.* The CORALIE survey for southern extrasolar planets. XVII. New and updated  
1018 long period and massive planets. *Astron. Astrophys.* **551**, A90 (2013).
- 1019 222. Mayor, M. *et al.* The CORALIE survey for southern extra-solar planets XII. Orbital solutions for 16  
1020 extra-solar planets discovered with CORALIE. *Astron. Astrophys.* **415**, 391-402 (2004).
- 1021 223. Mayor, M. *et al.* The HARPS search for southern extra-solar planets. XIII. A planetary system with  
1022 3 super-Earths (4.2, 6.9, and 9.2 M<sub>⊕</sub>). *Astron. Astrophys.* **493**, 639-644 (2009).
- 1023 224. Melendez, J. *et al.* The Solar Twin Planet Search. V. Close-in, low-mass planet candidates and  
1024 evidence of planet accretion in the solar twin HIP 68468. *Astron. Astrophys.* **597**, A34 (2017).
- 1025 225. Melo, C. *et al.* A new Neptune-mass planet orbiting HD 219828. *Astron. Astrophys.* **467**, 721-727  
1026 (2007).
- 1027 226. Meschiari, S. *et al.* The Lick-Carnegie Survey: Four new exoplanet candidates. *Astrophys. J.* **727**,  
1028 117 (2011).

- 1029 227. Minniti, D. *et al.* Low-Mass Companions for Five Solar-Type Stars From the Magellan Planet Search  
1030 Program. *Astrophys. J.* **693**, 1424-1430 (2009).
- 1031 228. Mitchell, D. S. *et al.* Precise radial velocities of giant stars. V. A brown dwarf and a planet orbiting  
1032 the K giant stars  $\tau$  Geminorum and 91 Aquarii. *Astron. Astrophys.* **555**, A87 (2013).
- 1033 229. Mocnik, T. *et al.* WASP-157b, a Transiting Hot Jupiter Observed with K2. Pub. Astron. Soc. Pacific  
1034 128, 124403 (2016).
- 1035 230. Mordasini, C. *et al.* The HARPS search for southern extra-solar planets. XXIV. Companions to HD  
1036 85390, HD 90156, and HD 103197: a Neptune analog and two intermediate-mass planets. *Astron.*  
1037 *Astrophys.* **526**, A119 (2011).
- 1038 231. Mortier, A. *et al.* New and updated stellar parameters for 71 evolved planet hosts. On the metallicity-  
1039 giant planet connection. *Astron. Astrophys.* **557**, A70 (2013a).
- 1040 232. Mortier, A. *et al.* New and updated stellar parameters for 90 transit hosts. The effect of the surface  
1041 gravity. *Astron. Astrophys.* **558**, A106 (2013b).
- 1042 233. Mortier, A. *et al.* The HARPS search for southern extra-solar planets. XXXIX. HD 175607, the most  
1043 metal-poor G dwarf with an orbiting sub-Neptune. *Astron. Astrophys.* **585**, A135 (2016).
- 1044 234. Moutou, C. *et al.* The HARPS search for southern extra-solar planets IV. Three close-in planets  
1045 around HD 2638, HD 27894 and HD 63454. *Astron. Astrophys.* **439**, 367-373 (2005).
- 1046 235. Moutou, C. *et al.* The HARPS search for southern extra-solar planets. XV. Six long-period giant  
1047 planets around BD -17 0063, HD 20868, HD 73267, HD 131664, HD 145377, and HD 153950.  
1048 *Astron. Astrophys.* **496**, 513-519 (2009).

- 1049 236. Moutou, C. *et al.* The HARPS search for southern extra-solar planets. XXVII. Seven new planetary  
1050 systems. *Astron. Astrophys.* **527**, A63 (2011).
- 1051 237. Moutou, C. *et al.* The SOPHIE search for northern extrasolar planets. VI. Three new hot Jupiters in  
1052 multi-planet extrasolar systems. *Astron. Astrophys.* **563**, A22 (2014).
- 1053 238. Moutou, C. *et al.* The HARPS search for southern extra-solar planets. XXXVII. Five new long-period  
1054 giant planets and a system update. *Astron. Astrophys.* **576**, A48 (2015).
- 1055 239. Naef, D. *et al.* The CORALIE survey for southern extrasolar planets. V. 3 new extrasolar planets.  
1056 *Astron. Astrophys.* **375**, 205-218 (2001).
- 1057 240. Naef, D. *et al.* The HARPS search for southern extra-solar planets IX. Exoplanets orbiting HD  
1058 100777, HD 190647, and HD 221287. *Astron. Astrophys.* **470**, 721-726 (2007).
- 1059 241. Naef, D. *et al.* The HARPS search for southern extrasolar planets XXIII. 8 planetary companions to  
1060 low-activity solar-type stars. *Astron. Astrophys.* **523**, A15 (2010).
- 1061 242. Nesvorný, D. *et al.* KOI-142, The King of Transit Variations, is a Pair of Planets near the 2:1  
1062 Resonance. *Astrophys. J.* **777**, 3 (2013).
- 1063 243. Neves, V. *et al.* Metallicity of M dwarfs. III. Planet-metallicity and planet-stellar mass correlations  
1064 of the HARPS GTO M dwarf sample. *Astron. Astrophys.* **551**, A36 (2013).
- 1065 244. Neveu-VanMalle, M. *et al.* WASP-94 A and B planets: hot-Jupiter cousins in a twin-star system.  
1066 *Astron. Astrophys.* **572**, A49 (2014).
- 1067 245. Neveu-Vanmalle, M., Queloz, D. & Anderson, D. Hot Jupiters with relatives: discovery of additional  
1068 planets in orbit around WASP-41 and WASP-47. *Astron. Astrophys.* **586**, A93 (2016).

- 1069 246. Niedzielski, A. *et al.* A Planetary-Mass Companion to the K0 Giant HD 17092. *Astrophys. J.* **669**,  
1070 1354-1358 (2007).
- 1071 247. Niedzielski, A., Goździewski, K. & Wolszczan, A. A Planet in a 0.6 AU orbit around the K0 giant  
1072 HD 102272. *Astrophys. J.* **693**, 276-780 (2009a).
- 1073 248. Niedzielski, A., Nowak, G., Adamów, M. & Wolszczan, A. Substellar-mass companions to the K-  
1074 Dwarf BD+14 4559 and the K-Giants HD 240210 and BD+20 2457. *Astrophys. J.* **707**, 768-777  
1075 (2009b).
- 1076 249. Niedzielski, A. *et al.* Tracking advanced planetary systems (TAPAS) with HARPS-N . I. A multiple  
1077 planetary system around the red giant star TYC 1422-614-1. *Astron. Astrophys.* **573**, A36 (2015a).
- 1078 250. Niedzielski, A *et al.* Three red giants with substellar-mass companions. *Astrophys. J.* **803**, 1-13  
1079 (2015b).
- 1080 251. Niedzielski, A. *et al.* Tracking advanced planetary systems (TAPAS) with HARPS-N. III. HD 5583  
1081 and BD+15 2375 - two cool giants with warm companions. *Astron. Astrophys.* **588**, A62 (2016a).
- 1082 252. Niedzielski, A. *et al.* Tracking advanced planetary systems (TAPAS) with HARPS-N IV. TYC 3667-  
1083 1280-1: The most massive red giant star hosting a warm Jupiter. *Astron. Astrophys.* **589**, L1 (2016b).
- 1084 253. Nowak, G *et al.* BD+15 2940 and HD 233604: Two giants with planets close to the engulfment zone.  
1085 *Astron. Astrophys.* **770**, 53-63 (2013).
- 1086 254. O'Toole, S. J. *et al.* New planets around three G dwarfs. *Astrophys. J.* **660**, 1636-1641 (2007).
- 1087 255. O'Toole, S. J. *et al.* Selection functions in doppler planet searches. *Mon. Not. Roy. Astron. Soc.* **392**,  
1088 641-654 (2009a).

- 1089 256. O'Toole, S. J. *et al.* A Neptune-mass Planet Orbiting the Nearby G Dwarf HD 16417. *Astrophys. J.*  
1090 **697**, 1263-1268 (2009b).
- 1091 257. Omiya, M *et al.* A massive substellar companion to the massive giant HD 119445. *Pub. Astron. Soc.*  
1092 *Japan* **61**, 825-831 (2009).
- 1093 258. Omiya, M *et al.* A Planetary Companion to the Intermediate-Mass Giant HD 100655. *Pub. Astron.*  
1094 *Soc. Japan* **64**, 34 (2012).
- 1095 259. Ortiz, M. *et al.* Kepler-432 b: a massive warm Jupiter in a 52-day eccentric orbit transiting a giant  
1096 star. *Astron. Astrophys.* **573**, L6 (2014).
- 1097 260. Ortiz, M. *et al.* Precise radial velocities of giant stars. IX. HD 59686 Ab: a massive circumstellar  
1098 planet orbiting a giant star in a 13.6 au eccentric binary system. *Astron. Astrophys.* **595**, A55 (2016).
- 1099 261. Peek, K. M. G. *et al.* Old, rich, and eccentric: Two Jovian planets orbiting evolved metal-rich stars.  
1100 *Pub. Astron. Soc. Pacific* **121**, 613-620 (2009).
- 1101 262. Pepe, F. *et al.* The HARPS search for southern extra-solar planets. I. HD 330075 b: A new ``hot  
1102 Jupiter''. *Astron. Astrophys.* **423**, 385-389 (2004).
- 1103 263. Pepe, F. *et al.* The HARPS search for southern extra-solar planets VIII. mu Arae, a system with four  
1104 planets. *Astron. Astrophys.* **462**, 769-776 (2007).
- 1105 264. Pepe, F. *et al.* The HARPS search for Earth-like planets in the habitable zone I. Very low-mass planets  
1106 around HD 20794, HD 85512, and HD 192310. *Astron. Astrophys.* **534**, A58 (2011).
- 1107 265. Pilyavsky, G. *et al.* A Search for the Transit of HD 168443b: Improved Orbital Parameters and  
1108 Photometry. *Astrophys. J.* **743**, 162 (2011).

- 1109 266. Perrier, C. *et al.* The ELODIE survey for northern extra-solar planets I. Six new extra-solar planet  
1110 candidates. *Astron. Astrophys.* **410**, 1039-1049 (2003).
- 1111 267. Queloz, D. *et al.* The CoRoT-7 planetary system: two orbiting super-Earths. *Astron. Astrophys.* **506**,  
1112 303-319 (2009).
- 1113 268. Quinn, S. N. *et al.* Two "b"s in the beehive: The discovery of the first hot Jupiters in an open cluster.  
1114 *Astrophys. J.* **756**, L33 (2012).
- 1115 269. Quinn, S. N. *et al.* HD 285507b: An eccentric hot Jupiter in the Hyades open cluster. *Astrophys. J.*  
1116 **787**, 27 (2014).
- 1117 270. Quinn, S. N. *et al.* Kepler-432: A red giant interacting with one of its two long-period giant planets.  
1118 *Astrophys. J.* **803**, 49 (2015).
- 1119 271. Rivera, P. *et al.* The Lick-Carnegie Exoplanet Survey: a Uranus-Mass Fourth Planet for GJ 876 in an  
1120 Extrasolar Laplace Configuration. *Astrophys. J.* **719**, 890-899 (2010).
- 1121 272. Rivera, P. *et al.* A Super-Earth Orbiting the Nearby Sun-like Star HD 1461. *Astrophys. J.* **708**, 1492-  
1122 1499 (2010).
- 1123 273. Robertson, P. *et al.* The McDonald Observatory Planet Search: New Long-period Giant Planets and  
1124 Two Interacting Jupiters in the HD 155358 System. *Astrophys. J.* **749**, 39 (2012a).
- 1125 274. Robertson, P. *et al.* A Second Giant Planet in 3:2 Mean-motion Resonance in the HD 204313 System.  
1126 *Astrophys. J.* **754**, 50 (2012b).
- 1127 275. Robertson, P. *et al.* Secretly eccentric: The giant planet and activity cycle of GJ 328. *Astrophys. J.*  
1128 **774**, 147 (2013).

- 1129 276. Robinson, S. E. *et al.* Two Jovian-mass planets in Earth-like orbits. *Astrophys. J.* **670**, 1391-1400  
1130 (2007).
- 1131 277. Rowan, D. *et al.* The Lick-Carnegie Exoplanet Survey: HD 32963—A new Jupiter analog orbiting a  
1132 Sun-like star. *Astrophys. J.* **817**, 104 (2016).
- 1133 278. Santos, N. C., Israelian, G. & Mayor, M. Spectroscopic [Fe/H] for 98 extra-solar planet-host stars.  
1134 Exploring the probability of planet formation. *Astron. Astrophys.* **415**, 1153-1166 (2004).
- 1135 279. Santos, N. C. *et al.* Spectroscopic metallicities for planet-host stars: Extending the samples. *Astron.*  
1136 *Astrophys.* **437**, 1127-1133 (2005).
- 1137 280. Santos, N. C. *et al.* ELODIE metallicity-biased search for transiting hot Jupiters. V. An intermediate-  
1138 period Jovian planet orbiting HD 45652. *Astron. Astrophys.* **487**, 369 (2008).
- 1139 281. Santos, N. C. *et al.* The HARPS search for southern extra-solar planets XXI. Three new giant planets  
1140 orbiting the metal-poor stars HD 5388, HD 181720, and HD 190984. *Astron. Astrophys.* **512**, A47  
1141 (2010).
- 1142 282. Santos, N. C. *et al.* The HARPS search for southern extrasolar planets. XXV. Results from the metal-  
1143 poor sample. *Astron. Astrophys.* **526**, A112 (2011).
- 1144 283. Santos, N. C. *et al.* An extreme planetary system around HD 219828. One long-period super Jupiter  
1145 to a hot-Neptune host star. *Astron. Astrophys.* **592**, A13 (2016).
- 1146 284. Sato, B. *et al.* A planetary companion to the G-type giant star HD 104985. *Astrophys. J.* **597**, 157-  
1147 160 (2003).
- 1148 285. Sato, B. *et al.* A Planetary Companion to the Hyades Giant ε Tauri. *Astrophys. J.* **661**, 527-531 (2007).

- 1149 286. Sato, B. *et al.* Planetary companions around three intermediate-mass G and K giants: 18 Delphini, ξ
- 1150 Aquilae, and HD 81688. *Pub. Astron. Soc. Japan* **60**, 539-550 (2008a).
- 1151 287. Sato, B. *et al.* Planetary companions to evolved intermediate-mass stars: 14 Andromedae, 81 Ceti, 6
- 1152 Lyncis, and HD 167042. *Pub. Astron. Soc. Japan* **60**, 1317-1326 (2008b).
- 1153 288. Sato, B. *et al.* Substellar Companions to Evolved Intermediate-Mass Stars: HD 145457 and HD
- 1154 180314. *Pub. Astron. Soc. Japan* **62**, 1063-1069 (2010).
- 1155 289. Sato, B. *et al.* Substellar companions to seven evolved intermediate-mass stars. *Pub. Astron. Soc.*
- 1156 *Japan* **64**, 135 (2012).
- 1157 290. Sato, B. *et al.* A double planetary system around the evolved intermediate-mass star HD 4732.
- 1158 *Astrophys. J.* **762**, 9 (2013a).
- 1159 291. Sato, B. *et al.* Planetary companions to three evolved intermediate-mass stars: HD 2952, HD 120084,
- 1160 and ω Serpentis. *Pub. Astro. Soc. Japan* **65**, 85 (2013b).
- 1161 292. Sato, B. *et al.* A pair of giant planets around the evolved intermediate-mass star HD 47366: Multiple
- 1162 circular orbits or a mutually retrograde configuration. *Astrophys. J.* **819**, 59 (2016).
- 1163 293. Ségransan, D. *et al.* The CORALIE survey for southern extrasolar planets. XVI. Discovery of a
- 1164 planetary system around HD 147018 and of two long period and massive planets orbiting HD 171238
- 1165 and HD 204313. *Astron. Astrophys.* **511**, A45 (2010).
- 1166 294. Ségransan, D. *et al.* The HARPS search for southern extra-solar planets. XXIX. Four new planets in
- 1167 orbit around the moderately active dwarfs HD 63765, HD 104067, HD 125595, and HIP 70849. *Astron.*
- 1168 *Astrophys.* **535**, A54 (2011).

- 1169 295. Setiawan, J. *et al.* Evidence of a sub-stellar companion around HD 47536. *Astron. Astrophys.* **398**,  
1170 19-23 (2003).
- 1171 296. Setiawan, J. *et al.* A substellar companion around the intermediate-mass giant star HD 11977. *Astron.*  
1172 *Astrophys.* **437**, 31-34 (2005).
- 1173 297. Soto, M. G. Jenkins, J. S. & Jones, M. I. RAFT - I. Discovery of new planetary candidates and  
1174 updated orbits from archival FEROS spectra. *451*, 3131-3144 (2015).
- 1175 298. Sousa, S. G. *et al.* Spectroscopic parameters for a sample of metal-rich solar-type stars. *Astron.*  
1176 *Astrophys.* **458**, 873-880 (2006).
- 1177 299. Sousa, S. G. *et al.* Spectroscopic parameters for 451 stars in the HARPS GTO Planet Search Program.  
1178 Stellar [Fe/H] and the frequency of exo-Neptunes. *Astron. Astrophys.* **487**, 373-381 (2008).
- 1179 300. Sousa, S. G. *et al.* Spectroscopic characterization of a sample of metal-poor solar-type stars from the  
1180 HARPS Planet Search Program. Precise spectroscopic parameters and mass estimation. *Astron.*  
1181 *Astrophys.* **526**, A99 (2011a).
- 1182 301. Sousa, S. G. *et al.* Homogeneous spectroscopic parameters for bright planet host stars from the  
1183 northern hemisphere. The impact on stellar and planetary mass. *Astron. Astrophys.* **576**, A94 (2015).
- 1184 302. Southworth, J. *et al.* Refined physical properties of the HAT-P-13 planetary system. *Mon. Not. Roy.*  
1185 *Astron. Soc.* **420**, 2580-2587 (2012).
- 1186 303. Sozzetti, A. *et al.* A massive planet to the young disc star HD 81040. *Astron. Astrophys.* **480**, 417-  
1187 424 (2006).
- 1188 304. Suarez Mascareno, A. *et al.* A super-Earth orbiting the nearby M-dwarf GJ 536. *Astron. Astrophys.*  
1189 **597**, A108 (2017).

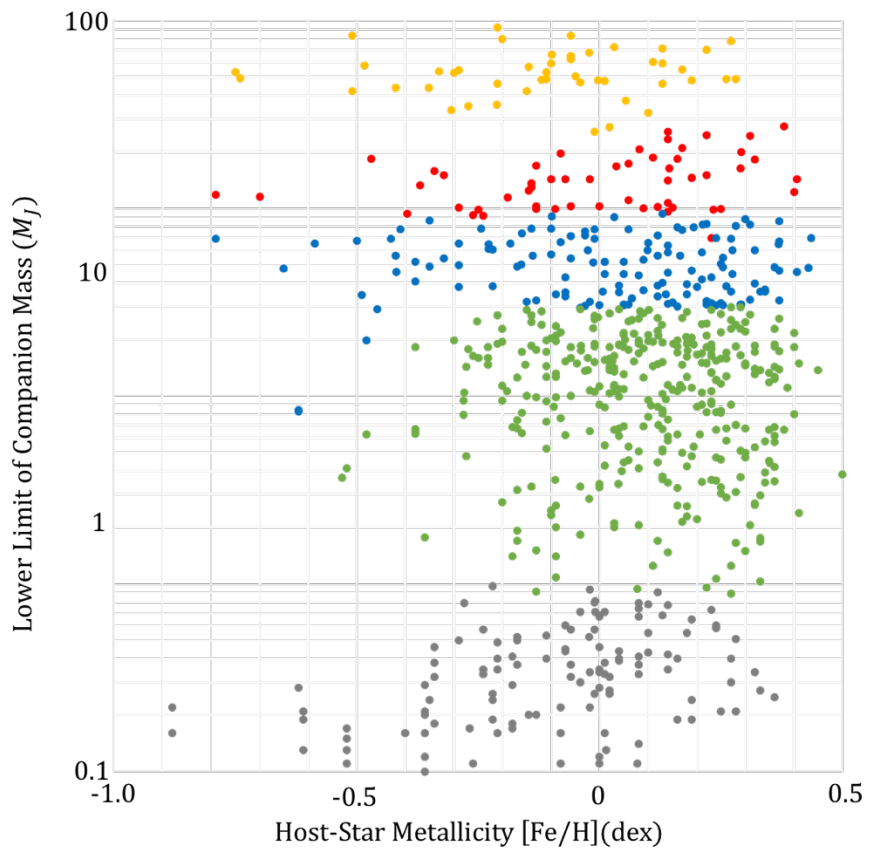
- 1190 305. Tamuz, O. *et al.* The CORALIE survey for southern extra-solar planets. XV. Discovery of two  
1191 eccentric planets orbiting HD 4113 and HD 156846. *Astron. Astrophys.* **480**, 33-36 (2008).
- 1192 306. Teske, J. K. *et al.* The Magellan PFS Search Program: Radial velocity and stellar abundance analysis  
1193 of the 360 AU, metal-poor binary “twins” HD 133131 A& B. *Astron. J.* **152**, 167 (2016).
- 1194 307. Tinney, C. G. *et al.* Four new planets orbiting metal-enriched stars. *Astrophys. J.* **587**, 423-428 (2003).
- 1195 308. Tinney, C. G. *et al.* The 2:1 Resonant Exoplanetary System Orbiting HD 73526. *Astrophys. J.* **647**,  
1196 594-599 (2006).
- 1197 309. Tinney, C. G. *et al.* The Anglo-Australian Planet Search. XX. A solitary ice-giant planet orbiting HD  
1198 102365. *Astrophys. J.* **727**, 103 (2011a).
- 1199 310. Tinney, C. G. *et al.* The Anglo-Australian Planet Search. XXI. A Gas-giant Planet in a One Year Orbit  
1200 and the Habitability of Gas-giant Satellites. *Astrophys. J.* **732**, 31 (2011b).
- 1201 311. Torres, G. Winn J. & Holman, M. J. Improved Parameters for Extrasolar Transiting Planets. *Astrophys.*  
1202 *J.* **677**, 1324-1342 (2008).
- 1203 312. Triaud, A. M. H. J. *et al.* Peculiar architectures for the WASP-53 and WASP-81 planet-hosting  
1204 systems. Accepted for publication in *Mon. Not. Roy. Astron. Soc.* (2017). Preprint at  
1205 <https://arxiv.org/abs/1612.04166>.
- 1206 313. Trifonov, T. *et al.* Precise radial velocities of giant stars. VI. A possible 2:1 resonant planet pair  
1207 around the K giant star η Ceti. *Astron. Astrophys.* **568**, A64 (2014).
- 1208 314. Tuomi, M. *et al.* Habitable-zone super-Earth candidate in a six-planet system around the K2.5V star  
1209 HD 40307. *Astron. Astrophys.* **549**, A48 (2013).

- 1210 315. Tsantaki, M. *et al.* Deriving precise parameters for cool solar-type stars. Optimizing the iron line list.  
1211 *Astron. Astrophys.* **555**, A150 (2013).
- 1212 316. Tsantaki, M. *et al.* Spectroscopic parameters for solar-type stars with moderate-to-high rotation. New  
1213 parameters for ten planet hosts. *Astron. Astrophys.* **570**, A80 (2014).
- 1214 317. Tuomi, M. A new cold sub-Saturnian candidate planet orbiting GJ 221. *Mon. Not. Roy. Astron. Soc.*  
1215 **440**, 1-5 (2014).
- 1216 318. Udry, S. *et al.* The CORALIE Survey for southern extra-solar planets. *Astron. Astrophys.* **390**, 267-  
1217 279 (2002).
- 1218 319. Udry, S. *et al.* Individual Detections to Statistical Properties. *Scientific Frontiers in Research on*  
1219 *Extrasolar Planets* **294** (2003a).
- 1220 320. Udry, S. *et al.* The CORALIE survey for southern extra-solar planets. X. A Hot Jupiter orbiting HD  
1221 73256. *Astron. Astrophys.* **390**, 267-279 (2003b).
- 1222 321. Udry, S. *et al.* The HARPS search for southern extra-solar planets V. A 14 Earth-masses planet  
1223 orbiting HD 4308. *Astron. Astrophys.* **447**, 361-367 (2006).
- 1224 322. Valenti, J. A. & Fisher, D. A. Spectroscopic properties of cool stars (SPOCS). I. 1040 F, G, and K  
1225 dwarfs from Keck, Lick, and AAT Planet Search Programs. *Astrophys. J. Suppl.* **159**, 141-166 (2005).
- 1226 323. Valenti, J. A. *et al.* Two exoplanets discovered at Keck Observatory. *Astrophys. J.* **702**, 989-997  
1227 (2009).
- 1228 324. Vogt, S. S. *et al.* Ten low-mass companions from the Keck precision velocity survey. *Astrophys. J.*  
1229 **568**, 352-362 (2002).
- 1230 325. Vogt, S. S. *et al.* Five New Multicomponent Planetary Systems. *Astrophys. J.* **632**, 638-658 (2005).

- 1231 326. Vogt, S. S. *et al.* A Super-Earth and Two Neptunes Orbiting the Nearby Sun-like Star 61 Virginis.  
1232 *Astrophys. J.* **708**, 1366-1375 (2010).
- 1233 327. Vogt, S. S. *et al.* A Four-planet System Orbiting The K0V Star HD 141399. *Astrophys. J.* **787**, 97  
1234 (2014).
- 1235 328. Vogt, S. S. *et al.* Six Planets Orbiting HD 219134. *Astrophys. J.* **814**, 12 (2015).
- 1236 329. Wang, S. X. *et al.* The discovery of HD 37605c and a dispositive null detection of transits of HD  
1237 37605 b. *Astrophys. J.* **761**, 46 (2012).
- 1238 330. Wang, L. *et al.* A long-period eccentric substellar companion to the evolved intermediate-mass star  
1239 HD 14067. *Pub. Astron. Soc. Japan* **66**, 1189 (2014).
- 1240 331. Winn, J. *et al.* The HAT-P-13 exoplanetary system: Evidence for spin-orbit alignment and a third  
1241 companion. *Astrophys. J.* **718**, 575-582 (2010).
- 1242 332. Wittenmyer, R. A. Endl, M. & Cochran, W. D. Long-Period Objects in the Extrasolar Planetary  
1243 Systems 47 Ursae Majoris and 14 Herculis. *Astrophys. J.* **654**, 625-632 (2007).
- 1244 333. Wittenmyer, R. A. *et al.* A Search for Multi-Planet Systems Using the Hobby-Eberly Telescope.  
1245 *Astrophys. J. Suppl.* **182**, 97-119 (2009).
- 1246 334. Wittenmyer, R. A. *et al.* The Pan-Pacific Planet Search. I. A Giant Planet Orbiting 7 CMa. *Astrophys.*  
1247 *J.* **743**, 184 (2011).
- 1248 335. Wittenmyer, R. A. *et al.* The Anglo-Australian Planet Search. XXII. Two New Multi-planet Systems.  
1249 *Astrophys. J.* **753**, 169 (2012).
- 1250 336. Wittenmyer, R. A. *et al.* Forever Alone? Testing Single Eccentric Planetary Systems for Multiple  
1251 Companions. *Astrophys. J. Suppl.* **208**, 2 (2013).

- 1252 337. Wittenmyer, R. A. *et al.* The Anglo-Australian Planet Search. XXIII. Two New Jupiter Analogs.
- 1253 *Astrophys. J.* **783**, 103 (2014a).
- 1254 338. Wittenmyer, R. A. *et al.* GJ 832c: A Super-Earth in the Habitable Zone. *Astrophys. J.* **783**, 103 (2014b).
- 1255
- 1256 339. Wittenmyer, R. A. *et al.* The Pan-Pacific Planet Search III: Five companions orbiting giant stars.
- 1257 *Mon. Not. Roy. Astron. Soc.* **455**, 1398-1405 (2016a).
- 1258 340. Wittenmyer, R. A. *et al.* The Anglo-Australian Planet Search XXV: A Candidate Massive Saturn
- 1259 Analog Orbiting HD 30177. Preprint at <https://arxiv.org/abs/1612.02072>.
- 1260 341. Wittenmyer, R. A. *et al.* The Pan-Pacific Planet Search. VI. Giant Planets Orbiting HD 86950 and
- 1261 HD 222076. *Astron. J.* **153**, 51 (2017).
- 1262 342. Wright, J. T. *et al.* The Jupiter Twin HD 154345b. *Astrophys. J.* **683**, L63 (2008).
- 1263 343. Wright, J. T. *et al.* Ten new and updated multiplanet systems and a survey of exoplanetary systems.
- 1264 *Astrophys. J.* **693**, 1084-1099 (2009a).
- 1265 344. Wright, J. T. *et al.* A Third Giant Planet Orbiting HIP 14810. *Astrophys. J.* **699**, 97-101 (2009b).
- 1266 345. Wright, J. T. *et al.* The California Planet Survey. III. A Possible 2:1 Resonance in the Exoplanetary
- 1267 Triple System HD 37124. *Astrophys. J.* **730**, 93 (2011).
- 1268 346. Zucker, S. *et al.* Multi-order TODCOR: Application to observations taken with the CORALIE echelle
- 1269 spectrograph. II. A planet in the system HD 41004. *Astron. Astrophys.* **426**, 695-698 (2004).
- 1270

1271



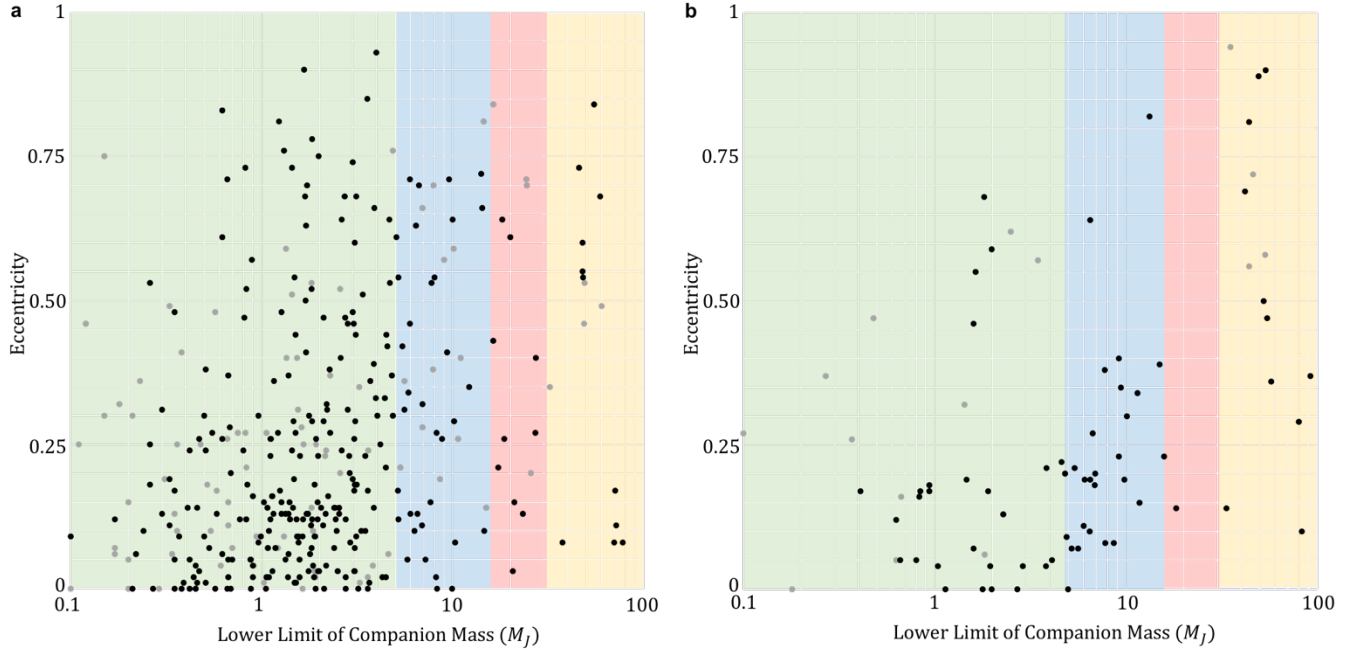
1272

1273 **Extended Data Figure 1. Most suitable model for all 722 samples.**

1274 **a,** The five-component model is selected as the best suited one for all 722 samples. The Gaussian mixture  
1275 models with the number of components ranging from 1 to 8 are fit to the distribution of the host-star  
1276 metallicities and companion masses. The best model is selected based on the Bayesian Information  
1277 Criterion (see Method section). The five-component model is selected from 55.0% of the 10000  
1278 calculations. In contrast, the other models are favored in fewer less than 20% of the calculations.

1279

1280



1281

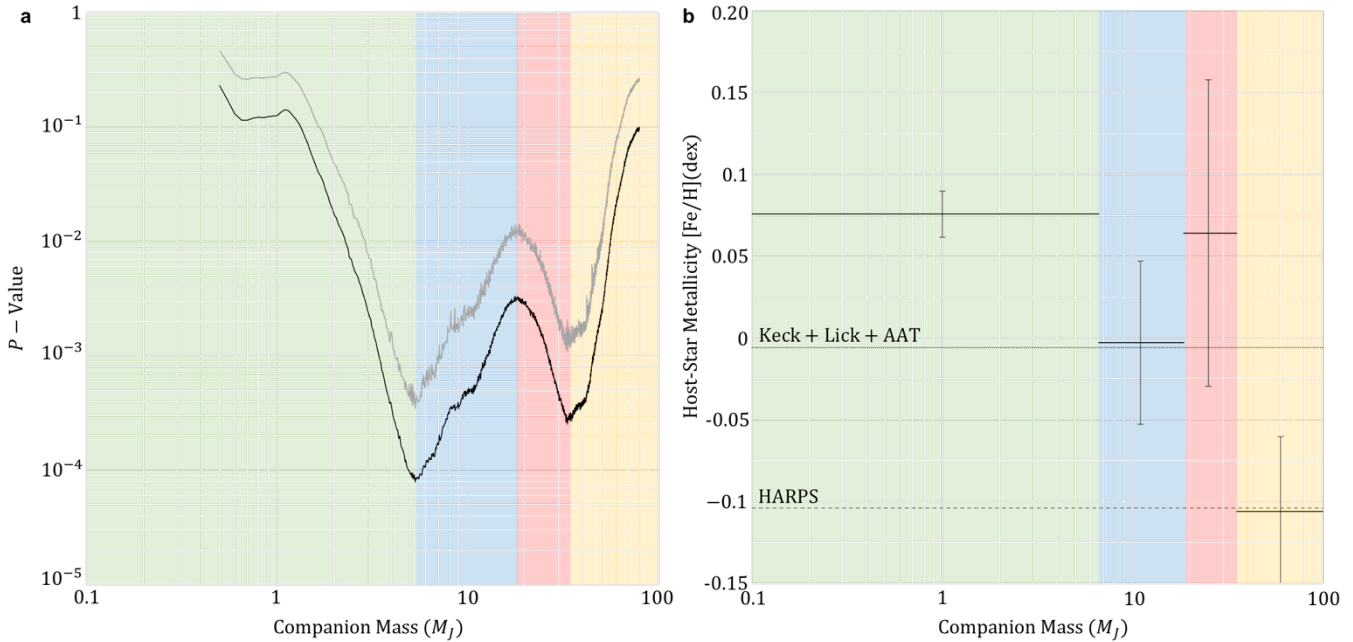
1282 **Extended Data Figure 2. Distributions of companion masses and eccentricities for two samples**  
 1283 **categorized according to host-star metallicity.**

1284 **a,** Companion mass and eccentricity distribution for the gaseous objects (black and grey dots) orbiting  
 1285 solar-metallicity and metal-rich stars ( $[{\rm Fe}/{\rm H}] \geq 0$ ). The black dots represent the samples, which can be  
 1286 detected by more than half of the radial-velocity observations around metal-poor stars (Method section).  
 1287 The green, blue, red and yellow areas indicate the four-mass regimes, intermediate-mass planets, massive  
 1288 planets, very massive planets and brown-dwarfs, respectively.

1289 **b,** Companion mass and eccentricity distribution for the gaseous objects (black and grey dots) orbiting  
 1290 metal-poor stars ( $[{\rm Fe}/{\rm H}] \leq -0.2$ ).

1291

1292



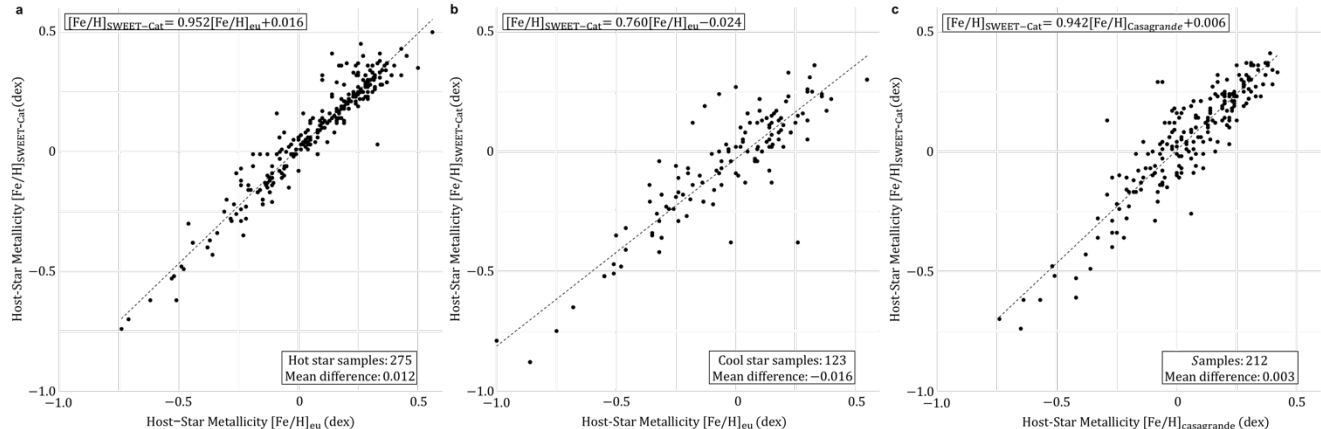
1293

1294 **Extended Data Figure 3: Multiple populations of gaseous objects in terms of the host-star**  
 1295 **metallicities considering uncertainty of orbital inclination.**

1296 **a,** Two-sample Anderson–Darling test result for the 589 gaseous objects extracted from all 722 samples.  
 1297 The lower boundary mass of the gaseous object is set to 0.1 Jupiter-mass. The *P*-values changes from 0.3  
 1298 to 80 Jupiter-mass in steps of 0.05 Jupiter-mass. The black line represents the mean *P*-value averaged over  
 1299 10000 calculations for each step. The grey line represents the 1-sigma upper limit of the *P*-value,  
 1300 considering the measurement errors on the host-star metallicities and the companion mass.

1301 **b,** Model for the 589 gaseous objects and mean host-star metallicities. The lower boundary mass is set to  
 1302 0.1 Jupiter-mass. The optimum model indicates that the 589 gaseous samples are divided into four bins:  
 1303  $0.1 \leq M_p < 6.6 M_J$ ,  $6.6 \leq M_p < 18.6 M_J$ ,  $18.6 \leq M_p < 35.3 M_J$ , and  $35.3 M_J \leq M_p$ , where  $M_J$  is Jupiter-  
 1304 mass. The mean metallicity and its standard deviation for each bin is shown. Dashed and dotted lines show  
 1305 the average metallicities for volume-limited samples of HARPS<sup>31</sup> and Keck, Lick, and AAT<sup>32</sup> radial  
 1306 velocity surveys, respectively.

1307



1308

1309 **Extended Data Figure 4. Correlation between metallicities in the SWEET-Cat, Exoplanet.eu, and**  
 1310 **Geneva–Copenhagen catalogues.**

1311 **a**, Metallicity correlation between Sweet-cat and Exoplanet.eu catalogues for hot stars with effective  
 1312 temperatures greater than 5000  $K$ . The number of samples in both catalogues is 275. The mean difference  
 1313 between the two metallicities is 0.012. The regression equation between the two samples is  
 1314  $[\text{Fe}/\text{H}]_{\text{casagrande}} = 0.952[\text{Fe}/\text{H}]_{\text{SWEET-Cat}} + 0.016$ .

1315 **b**, Metallicity correlation between Sweet-cat and Exoplanet.eu catalogues for cool stars with effective  
 1316 temperatures less than 5000  $K$ . The number of samples in both catalogues is 123. The mean difference  
 1317 between the two metallicities is -0.016. The regression equation between the two samples is  
 1318  $[\text{Fe}/\text{H}]_{\text{casagrande}} = 0.760[\text{Fe}/\text{H}]_{\text{SWEET-Cat}} - 0.024$ .

1319 **a**, Metallicity correlation between Sweet-cat and Geneva-Copenhagen catalogues. The number of samples  
 1320 in both catalogues is 275. The effective temperature of most of the samples is greater than 5000  $K$ . The  
 1321 mean difference between the two metallicities is 0.003. The regression equation between the two samples  
 1322 is  $[\text{Fe}/\text{H}]_{\text{casagrande}} = 0.942[\text{Fe}/\text{H}]_{\text{SWEET-Cat}} + 0.006$ .

1323

1324

1325 **Extended Data Table 1.** Parameters of stars hosting the 722 samples used in this study.

1326 Please see attached PDF document: ‘Extended\_Data\_Table1.pdf’.

1327

1328 **Extended Data Table 2.** Orbital parameters of the 722 samples used in this paper.

1329 Please see attached PDF document: ‘Extended\_Data\_Table2.pdf’.

1330

1331 **Extended Data Table 3.** Parameters of radial velocity observations of metal-poor ( $[Fe/H] \geq 0.2$ ) stars.

1332 Please see attached PDF document: ‘Extended\_Data\_Table3.pdf’.

1333

1334